Design Optimisation and Performance of a Simplified 5 MW Reluctance Synchronous Wind Generator

by

Jandré Dippenaar

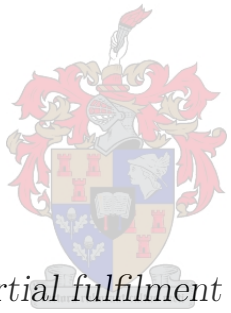

Thesis presented in partial fulfilment of the requirements for the degree of Master of Engineering (Electrical) in the Faculty of Engineering at Stellenbosch University

Supervisor: Prof. M.J. Kamper

March 2021

This work was financially supported by the Centre for Renewable and Sustainable Energy Studies at Stellenbosch University in South Africa and the Department of Science and Innovation (DSI) in South Africa.

Declaration

By submitting this thesis electronically, I declare that the entirety of the work contained therein is my own, original work, that I am the sole author thereof (save to the extent explicitly otherwise stated), that reproduction and publication thereof by Stellenbosch University will not infringe any third party rights and that I have not previously in its entirety or in part submitted it for obtaining any qualification.

Date: 2021/02/25 .....

Abstract

Design Optimisation and Performance of a Simplified 5 MW Reluctance Synchronous Wind Generator

J. Dippenaar

Department of Electrical and Electronic Engineering,
University of Stellenbosch,
Private Bag X1, Matieland 7602, South Africa.

Thesis: MEng (Electrical)

March 2021

Wind turbines are one of the solutions currently being implemented to address a globally increasing energy demand. Ongoing research, concerning every aspect of a wind turbine, aims to find better solutions in this field. One of these research aspects is the generator. This study investigates a 5 MW, 10-pole, 3-phase, medium speed, reluctance synchronous wind generator. These generators often make use of distributed flux-barriers in their rotors, with varying levels of complexity. However, in this thesis, a much simpler salient-pole rotor design is investigated that addresses a lack in the body of knowledge on simple, multi-megawatt reluctance synchronous generators (RSGs).

The salient-pole RSG is compared to a published equivalent RSG that has a typical flux-barrier rotor. In order to make this comparison, the design parameters of the salient-pole RSG are kept as close as possible to that of the flux-barrier RSG. Performance results are obtained by combining a FEM- and an optimisation package for the design optimisation of the salient-pole RSG. The FE results are verified with a second, independent FEM package.

From the performance results, a low power factor is clearly one of the weakest aspects of the salient-pole RSG design. In an attempt to improve this low power factor, a few modifications are made to the salient-pole rotor structure, based on rotor designs from the literature. These modifications include slitting, chamfering and tapering. The power factor is most improved by a fourth, more substantial, modification resulting in a split-pole RSG design. For this design, the rotor poles are split down the middle and separated by an

air-gap. Finally, suggestions are made for the physical construction of such a split-pole design, which is accompanied by a FE deformation analysis.

Uittreksel

Ontwerp Optimalisering en Vermoë van 'n Vereenvoudigde 5 MW Reluktansie Sinchrone Windgenerator

("Design Optimisation and Performance of a Simplified 5 MW Reluctance Synchronous Wind Generator")

J. Dippenaar

Departement Elektriese en Elektroniese Ingenieurswese,
Universiteit van Stellenbosch,
Privaatsak X1, Matieland 7602, Suid Afrika.

Tesis: MIng (Elektries)

Maart 2021

Windturbines is een van die oplossings wat tans geïmplementeer word om 'n wêreldwye toenemende energiebehoefte aan te spreek. Voortgesette navorsing rakende elke aspek van 'n windturbine, het ten doel om beter oplossings op hierdie gebied te vind. Een van hierdie navorsingsfokusse is die generator. Hierdie studie ondersoek 'n 5 MW, 10-pool, driefase, medium-spoed, reluktansie sinchrone windgenerator. Hierdie generators maak dikwels gebruik van verspreide vloedversperrings in die rotors, met verskillende vlakke van kompleksiteit. In hierdie tesis word 'n veel eenvoudiger speekpool rotor ontwerp ondersoek wat die gebrek aan kennis oor eenvoudige, multi-megawatt reluktansie sinchroongenerators (RSG's) aanspreek.

Die speekpool RSG word vergelyk met 'n gepubliseerde ekwivalente RSG wat 'n tipiese vloedversperringsrotor het. Ten einde hierdie vergelyking te tref, word die ontwerpparameters van die speekpool RSG so na as moontlik aan die van die vloedversperringsrotor-RSG gehou. Vermoë-resultate word verkry deur 'n FEMen 'n optimaliseringspakket te kombineer vir die ontwerp-optimalisering van die speekpool RSG. Die FE-resultate word bevestig met die resultate van 'n tweede, onafhanklike FEM-pakket.

Vanuit die vermoë-resultate is die lae arbeidsfaktor duidelik een van die swak aspekte van die speekpool RSG ontwerp. In 'n poging om hierdie lae arbeidsfaktor te verbeter, word 'n paar wysigings aangebring aan die speekpool rotorstruktuur, gebaseer op rotor-ontwerpe vanuit die literatuur. Hier-

die wysigings sluit in splitsing, afkanting en tapsafwerking. Die arbeidsfaktor word die beste verbeter deur 'n vierde, meer wesenlike aanpassing naamlik 'n gesplete-pool RSG ontwerp. Vir hierdie ontwerp word die rotorpool in die middel verdeel,geskei deur 'n luggaping. Laastens word voorstelle gemaak vir die fisiese konstruksie van so 'n gesplete-pool ontwerp, tesame met FE-vervormingsanalise.

Acknowledgements

I would like to express my sincere gratitude to the following people:

- Prof. Maarten Kamper. Thank you for being an example of a Godly man. You have embodied the following quote, attributed to Martin Luther: "The Christian shoemaker does his Christian duty not by putting little crosses on the shoes, but by making good shoes". You bring God glory in the way you pursue excellence and in the way you interact with people of all kinds. I will much sooner forget my research than my interactions with you.

- My wife and love of my life, Emma. We got married on 31 March 2019 - right in the middle of my thesis. Although this is partly why I took three years instead of two, your ongoing support is definitely why it didn't take four. I will never forget all the meals and words of encouragement when nights got late. I'm looking forward to showing this to our kids one day, God willing.

- My parents, Radie and Henriëtte Dippenaar. The fact that the child of a housing maintenance worker/handy-man and a home-B&B manager was able to get an undergrad engineering degree, much less a masters degree, is a testament to your love and dedication. I really love you and hope that I can transfer the virtues you have instilled in me to the generations to come.

- My friends and church family. There are too many to name. Even though life has stretched us apart somewhat, I want to thank *Die Maats* for all the encouragement, advice and interest in this thesis. Thank you for all the wisdom, laughs and for allowing me to do life with you.

- The EMLabs squad. What a diverse group of people! I really enjoyed getting to know each of you and learn from you. Thanks to Kenan for the help with the *Inventor* CAD and to Andrew for answering all my questions. I want to especially thank the bible study group. Thank you for the time spent studying the word, praying and discussing interesting questions. I will never forget the story Prof. told about the Chinese

researcher who, as an atheist, attended the group and eventually committed his life to Jesus and got baptised. My prayer is that all the members of the EMLabs group will come to know Jesus as their saviour.

- Jesus, my Lord and Saviour. Father, I know that throughout the process of completing this masters, I have wronged you. I know that I need your forgiveness and I am grateful that you extend it to me. Thank you, for bringing me through this process and for every thing that I have learnt through it. May I always bring you glory.

Dedications

Hierdie tesis word opgedra aan God.

"Lift up your eyes to the heavens, and look at the earth below; for the heavens will vanish like smoke, the earth will wear out like a garment, and its people will die like gnats. But My salvation will last forever, and My righteousness will never fail." - Isaiah 51:6

Presented Work

The work in this thesis has been presented in different papers at the following conferences:

1. J. Dippenaar and M. J. Kamper, "Simple Robust Rotor 5 MW Synchronous Reluctance Generator", *2020 IEEE Energy Conversion Congress and Exposition (ECCE)*, Detroit, MI, USA, October 2020.

2. J. Dippenaar and M. J. Kamper, "A Robust 5 MW Split-Pole Reluctance Synchronous Wind Generator", *2020 XXIV International Conference on Electrical Machines (ICEM)*, Gothenburg, Sweden, August 2020.

3. J. Dippenaar and M. J. Kamper, "A Simple 5 MW Split-Pole Reluctance Synchronous Wind Generator", *11th Renewable Energy Postgraduate Student Symposium*, Potchefstroom, South Africa, September 2020.

Contents

List of Figures

List of Tables

Nomenclature

Variables

A	Electrical loading	kA/m
A_{cu}	Active coppor area of a stator slot	m^3
A_{rms}	RMS current loading	A
B_g	Average peak-plateau flux density in the air-gap between the rotor pole and the stator core teeth	T
cp	Coil pitch in terms of the number of stator slots	
d_g	Air-gap diameter	m
d_i	Stator inner diameter	m
E_d, E_q	Steady-state, d- and q-axis EMF components	V
I_d, I_q	Steady-state, d- and q-axis stator currents	A
I_s	Space phasor of stator currents	A
I_{TP}	Total current in the magnetic field	A
J	Current density	A/m^2
J_s	RMS stator current density	A/m^2
k_A	Correction factor for chorded and fractional-slot windings	
k_d	Winding distribution factor	
$k_{e(2)}$	End-winding factor	
k_f	Stator slot fill factor	
$k_{p(2)}$	End-winding coil pitch factor	
k_r	Active slot factor	

L_d, L_q	d- and q-axis inductances	H
L_e	Endwinding leakage inductance	H
l_e	Average length of a winding end	m
l_s	Stack length	m
m	Number of phases	
n_a	Number of parallel winding circuits	
N_{s1}	Number of stator slots with coil layers of the same phase	
N_{s1}	Number of stator slots	
p	Number of pole pairs	
P_{core}	Core losses	W
P_{cu}	Stator copper losses	W
P_{in}	Mechanical shaft input power	W
P_{out}	Output power delivered to the convertor	W
q	Number of slots per pole per phase	
R_c	Core loss resistance, per phase	Ω
R_s	Stator resistance, per phase	Ω
t_c	Winding temperature	$^\circ C$
T_e	Electromagnetic developed torque	Nm
T_{mech}	Mechanical shaft input torque	Nm
V_2	Winding shape factor	
V_d, V_q	Steady-state, d- and q-axis stator voltages	V
V_s	Stator voltage space phasor	V
W	Number of series turns per phase	
x_i	Scaled optimisation design variables	
z	Number of conductors per stator slot	
z_i	Unscaled optimisation design variables	

T_{avg}	Average torque	Nm
T_{max}	Maximum torque	Nm
T_{min}	Minimum torque	Nm
T_{ripple}	Torque ripple	Nm

Greek Symbols

α	Skew angle	rad
η	Efficiency	
λ_d, λ_q	d- and q-axis flux linkages	Wb
ω_e	electrical angular velocity	rad/s
ω_m	mechanical angular velocity	rad/s
ϕ	Power factor angle	rad
ρ_t	Resistivity of copper at a temperature of t	Ωm
θ	Current angle	rad
θ_r	Mechanical rotor pole pitch	rad
θ_s	Magnetic pole pitch	rad

Abbreviations

2D	Two dimensional
AC	Alternating current
CAD	Computer aided design
d-axis	Direct axis
DTU	Technical University of Denmark
EESG	Electrically excited synchronous generator
Eff	Efficiency
FE	Finite element
FEM	Finite element method
GE	General Electric
IEEE	Institute of Electrical and Electronics Engineers

mm	Millimeter
MMFD	Modified Method of Feasible Directions
MW	Megawatt
NSGA-II	Non-dominant sorting genetic algorithm
PF	Power factor
PMSG	Permanent magnet synchronous generator
q-axis	Quadrature axis
r/min	Rotations per minute
R&D	Research and development
RSG	Reluctance synchronous generator
RSM	Reluctance synchronous machine
SEMFEM	Stellenbosch Electrical Machines Finite Element Method
Sim	Simulation
SLP	Sequential Linear Programming
SP	Slot pitch
SRG	Switched reluctance generator

Chapter 1

Introduction

The world is in search of more sustainable and environmentally friendly solutions to meet the need of a growing energy demand. One of these proposed solutions is wind energy. Wind energy has recently experienced remarkable growth, with offshore technologies alone growing 30% per year from 2010 to 2018 [1]. The size of both on- and offshore turbines are increasing, with *offshore* turbines breaking the 10 MW mark and manufacturers such as *GE*, *Vestas* and *Siemens Gamesa* all offering *onshore* turbines reaching 5 MW.

Furthermore, there is a growth in the use of full-rated power converters as an interface between the generator and the power grid in renewable energy systems such as wind- and hydro-energy generation [2], [3]. With the use of these power converters maximum torque per ampere and adjustable speed can be achieved. The generators can be connected to the turbines either directly or via gearboxes. The direct-drive solution can be associated with an increase in generator mass, while a high-speed gearbox can decrease reliability. As a result, the medium-speed gearbox has drawn some attention for wind generation systems, as a well-balanced trade-off between mass and reliability [2], [4].

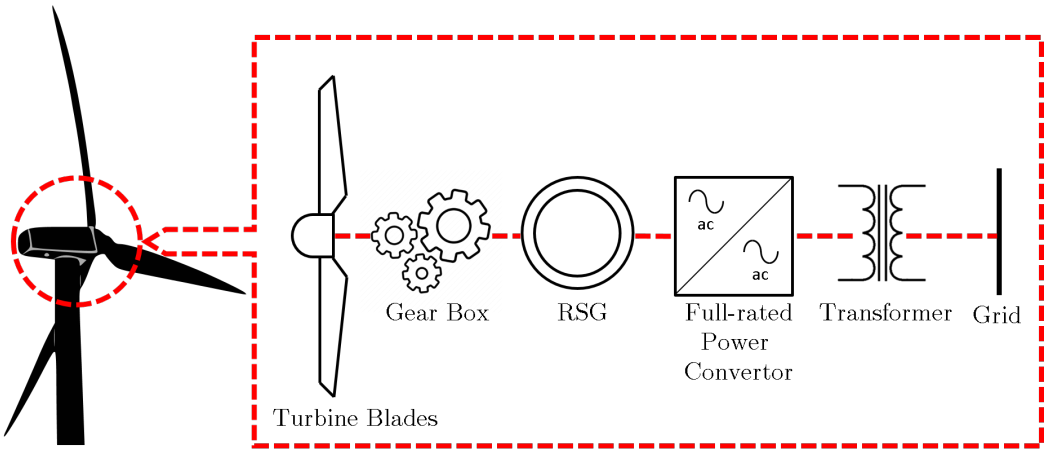

Figure 1.1: The wind-energy generation system studied in this thesis.

As an example, the *Vestas V164-9.5* MW turbine has a rated speed of 400 r/min, a maximum speed of 536 r/min and uses a 3 stage planetary differential gearbox with a 1:38.03 gear ratio [5]. The medium-speed range for wind generators is, in general, taken as between 100- and 500 r/min.

Figure 1.1 shows the wind energy generation system that is studied in this thesis. It consists of turbine blades that is connected to the generator via a medium speed gearbox. The generator feeds electricity to the grid via a transformer, after passing through a full-rated power converter. We will mainly focus our research attention on the generator component of the wind energy generation system.

There is an increased focused on non-permanent magnet generator solutions, even though permanent magnet generators offer good power density and efficiency. Magnets are typically expensive, and even the more affordable ferrite magnets run the risk of demagnetization, making a non-permanent magnet solution more robust. Non-permanent magnet generators include, inter alia, induction generators, wound-rotor synchronous generators and switched reluctance generators (SRGs). The use of reluctance synchronous generators (RSGs) for wind energy generation has attracted attention at a 5 MW power level, as shown in work done by Roshanfekr [6] and Howard [7]. The conductorless iron rotor, good efficiency and standard converter make the RSG very attractive to use. Considering the trends mentioned, our focus for this thesis is therefore on the RSG designed for a medium-speed wind generator at 5 MW.

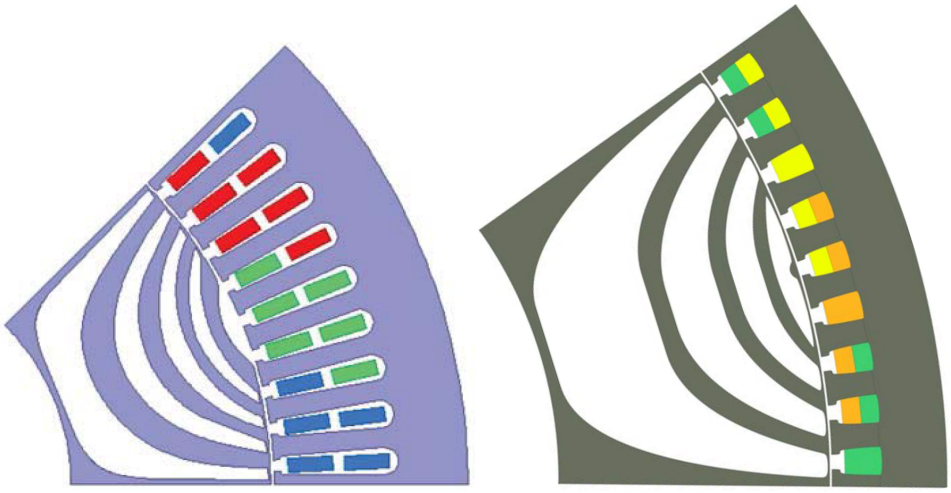

(a) (b)

Figure 1.2: Cross-sections of 5 MW designs of (a) the 8-pole generator of Roshanfekr and (b) the 10-pole generator of Howard.

1.1 Background of the RSG

The reluctance synchronous machine (RSM) operates on the fundamental principle that a piece of iron in a magnetic field will align itself in such a way that it offers the path of least magnetic reluctance for the magnetic flux to pass through the metal. Magnetic reluctance can be thought of as analogous to resistance in electrical circuits. In essence, reluctance is the opposition to magnetic flux. If the magnetic field thus rotates around the metal, the metal will rotate along with it, continually serving as the path of least magnetic reluctance. This is illustrated in Figure 1.3 [8] with a very simple two-sided salient-pole rotor. For RSMs, a rotating magnetic field is typically created around the rotor via a multi-phase, (usually consisting of three phases) AC, stator winding. Over time, the RSM has undergone significant developments and changes.

Kamper [9] offers a comprehensive summary of the history behind the development of the reluctance synchronous machine. He, and others ([10], [11]) note that a remarkable paper by Kostko [12] in 1923 marked the start of the modern flux-barrier RSMs we have today, as shown in Figure 1.4a with *ABBs* commercial RSM solution. Kostko's rotor is shown in Figure 1.4b. Before the flux-barrier rotor RSM, there was the *salient-pole* rotor reluctance machine, which date even further back. Kostko notes that "The reaction synchronous motor in its present form (salient-pole rotor without field coils) is one of the oldest types of electric motors, antedating the induction motor by many years.". A typical salient-pole rotor is shown in Figure 1.4c as part of a switched reluctance machine, with its characteristic rotor protrusions referred

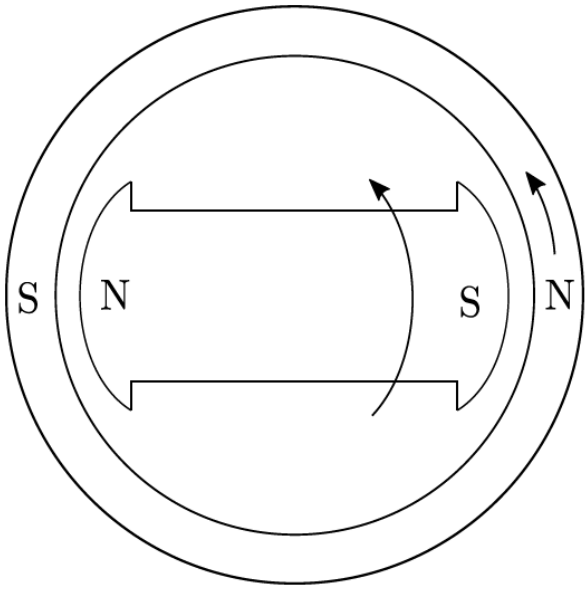

Figure 1.3: A demonstration of the operating principle of the RSM.

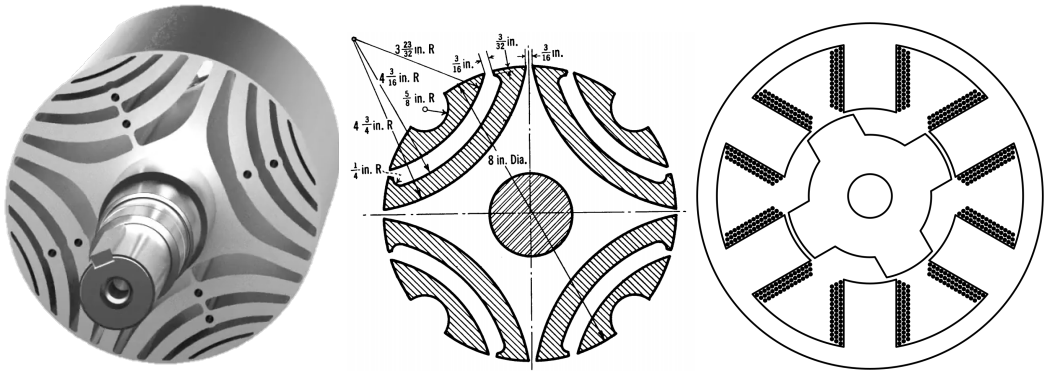

(a) (b) (c)

Figure 1.4: Cross-sections of RSM designs showing (a) the commercially available RSM from *ABB* (b) an early flux-barrier type rotor by Kostko from 1923 and (c) a typical salient-pole rotor, switched reluctance machine.

to as salient-poles.

In the RSGs of both Roshanfekr [6] and Howard [7], typical distributed flux barriers are used in the design of the rotors, which can be seen in Figure 1.2. It is interesting how the designs differ. A potential problem in both these designs is the mechanical strength of the rotors. It is shown by Taghavi and Pillay [13] that the thin ribs at the end of the rotor flux barriers are especially susceptible to mechanical failure. Assuming mechanical feasibility, as is done by Howard, can thus be problematic.

The vast majority of research surrounding RSM rotors consider these distributed flux barrier rotor designs. In this thesis we return to a simpler, salient-pole rotor design for the 5 MW, medium-speed RSG.

1.2 Problem statement

Research concerning typical flux-barrier RSGs in the multimegawatt range is scarce. Research concerning *salient-pole* RSGs in the multi-megawatt range is non-existent. Yet, the salient-pole design is a much simpler and more robust design. It could potentially decrease manufacturing costs and offer a smaller chance of system failure due to its increased mechanical strength. It is a worthwhile endeavour to investigate how an optimum salient-pole RSG compares to an optimum flux-barrier RSG. We lay out the research problem as follows:

- We do not know how a simpler, salient-pole RSG compares to a multi-megawatt RSG, for wind generation.
- Simplicity offers improved robustness at a smaller manufacturing cost. So if a simpler design provides similar performance to a more complex design, why use a more complex solution?

- Therefore, to solve the problem and fill the gap in knowledge, we need a fair comparison of a simplified RSG with an equivalent distributed flux-barrier RSG.

1.3 Approach to the Problem

The problem is identified as a lack of knowledge regarding the performance of simple, salient-pole RSGs in the megawatt range - could a simple RSG perform comparatively to a more complex, distributed flux barrier RSG? To answer this question the following approach is followed:

- Select a published multi-megawatt RSG to compare the simplified RSG with.
- Keep the design parameters of the simplified RSG similar to the published RSG, making allowance for structural differences.
- Set up a model for the simplified RSG, use the model in a FEM simulation of the RSG and verify the simulation results with a second FEM package.
- Optimise the RSG.
- Identify problem areas in the performance of the optimum RSGs and implement minor modifications to the design in order to address those problem areas.
- Compare the simplified RSG with a published equivalent distributed flux-barrier RSG.

The published RSG that is selected for comparison is that of Howard [7], [14]. The parameters of the salient-pole RSG, like the pole number and total volume, are kept as close as possible to that of Howard. There are some notable exceptions. A lower current density of less than $J = 2$ A/mm^2 and an electrical loading less than $A = 80$ kA/m (in order to have feasible AJ values), are used in the design in order for the machine to operate under air cooling. Although a higher current density would likely increase power output, it is also associated with higher temperatures. In order to avoid over-saturating the machine and to keep the operating temperatures low enough for air cooling, a lower current density is chosen. A higher fill factor of 0.6 is chosen, which is consistent with recommendations by Sethuraman et al. [15] and Boldea [16]. A slightly more conservative air-gap of 3 mm is also implemented. A different winding - a distributed fractional-slot winding - is implemented to decrease a high torque ripple; this will be discussed in Chapter 3.

Using these parameters, the resulting salient-pole machine is modelled and then solved with a FEM package. It is subsequently optimised in Chapter 4, to

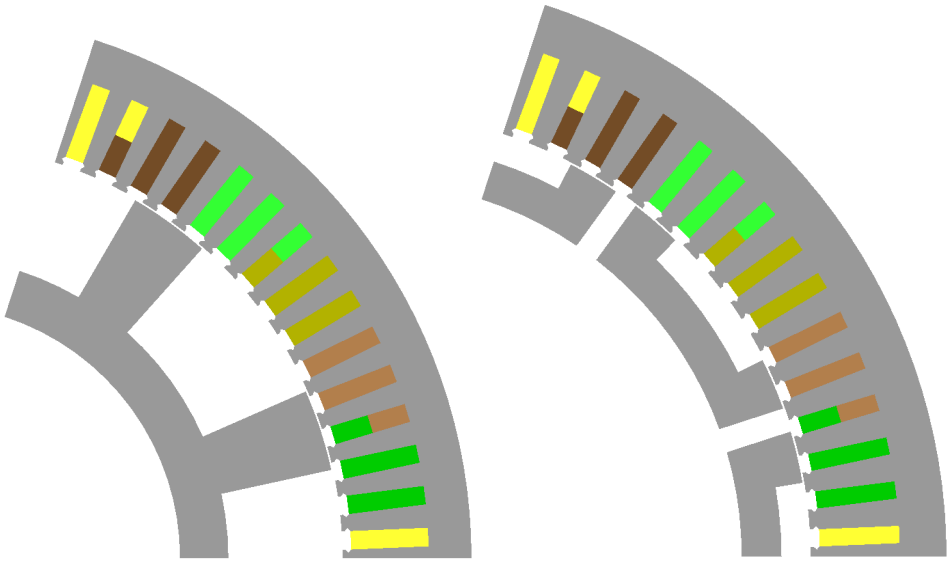

(a) (b)

Figure 1.5: Cross-sections of the RSG designs presented in this thesis showing (a) a salient-pole RSG and (b) a split-pole RSG.

give a RSG of the type shown in Figure 1.5a. A low power factor is identified as the Achilles heel of this RSG, as it is about 37% lower than that of Howard. In an attempt to increase the power factor, various changes are made to the salient-pole rotor design, presented in Chapter 5.

A further and more dramatic alteration is discussed in Chapter 6, involving a split-pole RSG. Flux barriers can be present in various quantities and have different geometries ranging from incredibly complex [17], to fairly simple [18]. The split-pole RSG involves utilising the flux barrier concept by splitting the rotor poles, in order to limit the q-axis flux linkage and increase the d-axis flux linkage, as shown in Figure 1.5b. This is done by Constancias et al. for an outer-rotor RSM [19]. Finally, the different salient-pole designs and improvements are contrasted to that of Howard in Chapter 7, in order to draw conclusions and make recommendations.

1.4 Thesis layout

To summarise, the layout of this thesis is as follows:

- **Chapter 1:** The rationale behind studying a simplified 5 MW salient-pole RSG is presented here, along with the approach that will be used to compare it with a published equivalent flux-barrier RSG.
- **Chapter 2:** In this chapter, the RSG is mathematically modelled and the equations for calculated performance is described.

- **Chapter 3:** The RSG model equations of Chapter 2 are needed for a FE-simulation. In this chapter, the simulation process which use these equations is explained and the simulation of a few techniques used to reduce the torque ripple of the RSG is also discussed.
- **Chapter 4:** After the process is in place to simulate the RSG, an optimum design has to be found. This chapter explains how the FE-simulation is integrated into the optimisation process.
- **Chapter 5:** This chapter displays the results of the salient-pole RSG design optimisation. In an attempt to improve the power factor, the rotor is modified through chamfering, slitting and tapering, the results of which are also shown in this chapter
- **Chapter 6:** As another attempt to increase the power factor, in this chapter the results of splitting the poles of the salient-pole RSG is shown. Additionally, recommendations for physical construction is made and supported with a brief deformation analysis.
- **Chapter 7:** Finally, the thesis concludes by highlighting some key points, mentioning some limitations and making some recommendations for future work.

Chapter 2

Modelling

In this chapter, we discuss how the real-world components of the RSG is modelled analytically so that we can arrive at a system of computational equations. These equations, along with a FEM analysis, enables us to calculate the theoretical machine performance, which in turn enables us to optimise the design.

2.1 dq Equivalent Circuits

In order to arrive at a system of basic computational equations, the key components of the RSG is represented in an equivalent electrical circuit. This is done in accordance with classical dq theory. The resultant equivalent circuit is shown in Figure 2.1. The dq transformation is used to represent the machine equations in the synchronously-rotating reference frame with respect to the rotor. We will assume a balanced system and therefore the 0-component, resulting from the dq transformation, is absent.

The equations are derived as if the machine is operating in motor mode. To operate as a generator, negative q-axis current is supplied, as Figure 2.2 illustrates. Figure 2.2 also shows the power factor angle, as represented by ϕ, and the current angle, under converter control, as represented by θ. The RSG has no rotor field-component and the equations for the d- and q-axis supply voltages under steady state conditions are,

$$V_d = R_s I_{d1} - \omega_e \lambda_q - L_e I_{q1} \omega_e, \tag{2.1}$$

$$V_q = R_s I_{q1} + \omega_e \lambda_d + L_e I_{d1} \omega_e. \tag{2.2}$$

In (2.1) and (2.2), ω_e is the electrical angular velocity, R_s is the stator winding resistance and L_e is the end-winding leakage inductance, which is calculated with (2.19) and explained later in this chapter. The d- and q-axis flux linkage values, given by λ_d and λ_q, include both the main flux and the leakage flux of the generator.

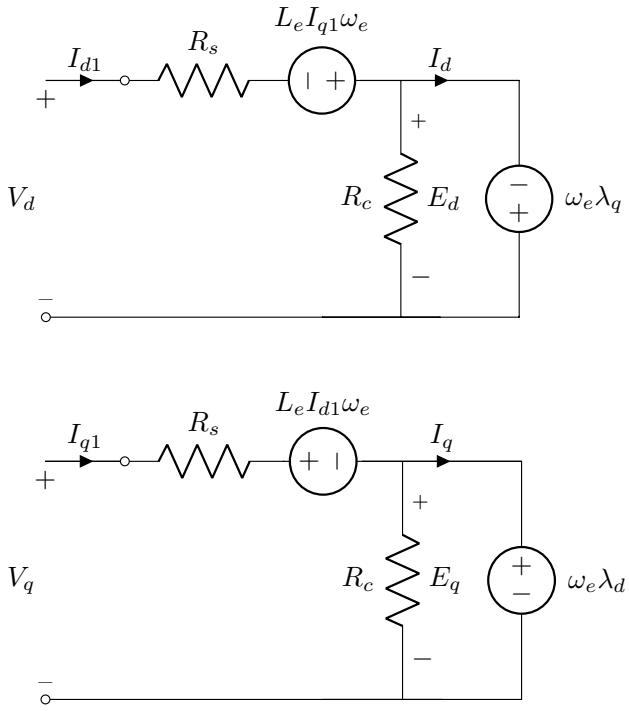

Figure 2.1: Equivalent dq circuits of the RSG.

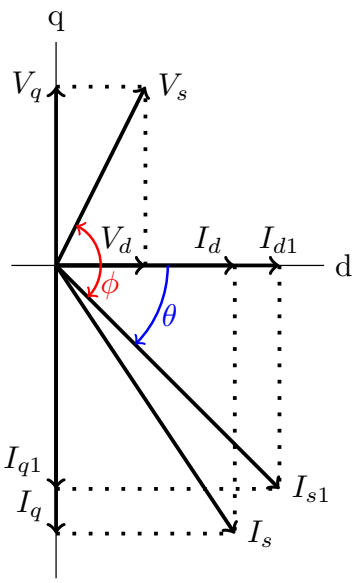

Figure 2.2: Space phasor diagram of the RSG.

The variables in this analytical analysis have been defined in a frame of reference that rotates at the electrical angular velocity given by,

$$\omega_e = \frac{d\theta_e}{dt}. \tag{2.3}$$

It relates to the speed of mechanical rotation as follows,

$$\omega_e = \frac{poles}{2}\omega_m. \tag{2.4}$$

The speed voltages are given by,

$$E_d = -\lambda_q \omega_e, \tag{2.5}$$

$$E_q = \lambda_d \omega_e. \tag{2.6}$$

The d- and q-axis inductances are determined by

$$L_d = \frac{\lambda_d}{I_d}, \tag{2.7}$$

$$L_q = \frac{\lambda_q}{I_q}. \tag{2.8}$$

The d- and q-axis supply currents then become,

$$I_{d1} = I_d + \frac{E_d}{R_c}, \tag{2.9}$$

$$I_{q1} = I_q + \frac{E_q}{R_c}. \tag{2.10}$$

The effect of the core losses are taken into account by R_c, the core resistance, in the equivalent circuits of Figure 2.1 and is determined by,

$$R_c = \frac{3E_a^2}{P_{core}}, \tag{2.11}$$

where E_a is the RMS value of the speed voltages (E_d, E_q) and given by

$$E_a = \sqrt{\frac{1}{2}(E_d^2 + E_q^2)}. \tag{2.12}$$

The rms amplitude of the stator voltage is given by,

$$V_s = \sqrt{\frac{V_d^2 + V_q^2}{2}}. \tag{2.13}$$

The rms amplitude of the stator current is,

$$I_s = \sqrt{\frac{I_{d1}^2 + I_{q1}^2}{2}}. \tag{2.14}$$

The torque acting to decelerate the rotor of the RSG is given by,

$$T_e = \frac{3}{4}p(\lambda_d I_q - \lambda_q I_d). \tag{2.15}$$

2.2 Copper Losses and Stator Winding Resistance

As laid out in [9], the resistance of the copper windings in the stator is calculated with,

$$R_s = \frac{2W\rho_t(l_s + l_e)}{n_a \frac{A_{cu}}{z}}, \tag{2.16}$$

where the symbols used in eq. (2.16) are described below:

W	=	Number of series turns per phase
ρ_t	=	Resistivity of copper
l_s	=	Stack length of the motor
l_e	=	Average length of a winding end
n_a	=	Number of parallel winding circuits
A_{cu}	=	Active copper area per stator slot
z	=	Number of conductors per stator slot

The average length of a winding end, l_e, is calculated with the approximation given by [14] where a semi-circular end-winding approximation is used. The resistivity of copper at winding temperature t_c is given by,

$$\rho_t = \rho_{20}[1 + Y_t(t_c - 20)], \tag{2.17}$$

with $\rho_{20} = 17\text{x}10^{-9}$, $Y_t = 0.0039/^o\text{C}$ and $t_c = 75^o\text{C}$.

With the stator winding resistance known, the stator copper losses can be determined by,

$$P_{cu} = 3I_{s1}^2 R_s. \tag{2.18}$$

2.3 End-winding Leakage Inductance

Once again, [9] is consulted to calculate the end-winding leakage inductance for elliptically shaped winding ends and is given by,

$$L_e = md_i \frac{V_2}{2\pi} \left(\frac{W k_d k_{p(2)}}{p} \right)^2 k_{e(2)} \times 10^{-8} \text{ H}, \tag{2.19}$$

where the symbols used in eq. (2.19) are described below, and $V_2 = 1180$ and $k_{e(2)} = 0.785$.

m	=	Number of phases
d_i	=	Stator inner diameter
V_2	=	Shape factor
W	=	Number of turns in series, per phase
p	=	Number of pole pairs
$k_{e(2)}$	=	End-winding factor for 2 pole pairs

Furthermore, the winding distribution factor is found by

$$k_d = \frac{sin(\frac{\pi}{6})}{qsin(\frac{\pi}{6q})}, \tag{2.20}$$

with q as the number of stator slots. The equation for the end-winding coil pitch factor is given by

$$k_{p(2)} = \frac{3sin(\frac{\pi cp}{6q})}{(4 - (\frac{cp}{3q})^2)} + sin\left(\frac{\pi cp}{6q}\right), \tag{2.21}$$

with cp as the coil pitch in terms of the number of stator slots.

2.4 Core Losses

A modified version of Steinmetz's core loss equation is used to determine the core losses:

$$P_{core} = cf_1^x(B_{tooth}^y M_{tooth} + B_{yoke}^y M_{yoke})k_{exp} \tag{2.22}$$

The Steinmetz coefficients are c, x and y and can be found by measurements and loss frequency curves at the fundamental supply frequency, f_1. The parameters B_{tooth} and B_{yoke} are the maximum flux densities in the tooth and yoke respectively, obtained from the FEM software. M_{tooth} and M_{yoke} are the masses of the teeth and the yoke respectively. This calculated value, P_{core}, is used to determine the core resistance in eq. (2.11).

2.5 Power and Efficiency

The equations for power generated from the RSG are described in terms of the working of a wind turbine, with the input power coming from the turning of the blades connected to the generator shaft via a gearbox. Generated power will have a negative calculated value, as the model has been set up with positive current flowing into the terminals. The power generated from the turning of the shaft is

$$P_{in} = T_{mech}\omega_m. \tag{2.23}$$

Looking at the model, the input power is also given by,

$$P_{in} = \frac{3}{2}\left(E_d I_d + E_q I_q\right). \tag{2.24}$$

The core losses, and copper losses decrease the power converted from mechanical to electrical form. These losses are,

$$P_{loss} = P_{core} + P_{cu} \tag{2.25}$$

Friction and windage losses, and stray losses are ignored in order to simplify the analysis and because they are typically quite low. Any losses due to the inclusion of a medium-speed gearbox in the drive-train is also ignored, as well as any losses in the generator due to inverter switching.

The power output from generation activity is given by,

$$P_{out} = P_{in} + P_{loss}. \tag{2.26}$$

Because the equations are set up in motor mode using negative q-axis current, the generated input power is negative. Adding the positive losses to it decreases the generated output power. The power output from generation activity is also given by,

$$P_{out} = -3V_s I_s \times PF. \tag{2.27}$$

The power factor is given by,

$$PF = cos(\phi), \tag{2.28}$$

where ϕ is given by,

$$\phi = atan\left(\frac{V_q}{V_d}\right) - atan\left(\frac{I_{q1}}{I_{d1}}\right). \tag{2.29}$$

Finally, the efficiency is given by,

$$\eta = \frac{P_{out}}{P_{in}} \times 100\%. \tag{2.30}$$

Chapter 3

FEM Simulation and Calculation

The equations that model the RSG are described in Chapter 2. These equations are used to calculate the performance of the RSG. However, before the performance can be calculated, a FEM simulation and calculation is done to determine the key values used in the performance calculation. This chapter describes how the FEM simulation and calculation is approached, using an in-house package, called *SEMFEM*. The results obtained from *SEMFEM* is then verified with a commercial FEM package called *Ansys Maxwell*. Additionally, this chapter describes two torque ripple reduction methods employed within the *SEMFEM* simulation, namely the use if a distributed fractional-slot winding and skewing the rotor.

3.1 Simulation

Various packages are available for designers and researchers to use in the modelling of electrical machines. Among these, are free tools like *MotorAnalysis* [20], *QuickField* [21] and *FEMM* [22]. There are also well-known commercial tools like *MATLAB*, *Ansys Maxwell* [23], *JMAG* [24], *MagNet* [25] and *COMSOL* [26]. Finally, there are some lesser known commercial tools like *MagneForce* [27] and *EMS* [28].

Within the electrical machines research group at Stellenbosch University, *SEMFEM* has gained popularity for its short simulation time and versatility, without sacrificing on accuracy. This package is thus selected for use and its results are verified with one of the commercial FEM simulation solutions, namely *Ansys Maxwell*.

3.1.1 SEMFEM

The *SEMFEM* package is an acronym for the Stellenbosch Electrical Machines Finite Element Method. It was first developed in 2011 by Gerber [29],[30] and has been continuously improved since. *SEMFEM* is an expansion and

improvement of what is known as *the Cambridge package*. It performs 2D, time-stepped finite element simulations. The functionality that was added by *SEMFEM* includes:

- The modelling of machines with more than one air-gap.
- The modelling of linear machines with tubular, axisymmetric topologies.
- The introduction of parallelisation for the FEM simulation and the optimisation program, in order to make the numerical optimisation process faster.

These improvements, amongst others, make *SEMFEM* a versatile and computationally fast machine simulation tool. Although it is comprehensive, it does not have all of the bells and whistles of some modern, commercial FEM tools. As a result, it is a focused tool that is built for speed.

The user interacts with *SEMFEM* using a Python script. The *SEMFEM* documentation [31] describe the fundamentals of the package well and it can be summarised as follows.

Typically, the first step of the simulation process is to "draw" the machine by specifying cartesian and polar coordinates in the script. The FEM simulation is then configured by specifying parameters like the number of air-gaps, the stack length, symmetry, boundary conditions, material characteristics, the current input, the winding parameters and the number of time-steps. The machine is subsequently meshed, based on the drawing, and a solver is invoked. *SEMFEM* has the useful ability to display these drawn and meshed machines visually. The FEM simulation and calculation then produce output values, the most important of these being the torque and flux linkages.

We follow this process for the machines in Figure 3.1 and, in order to verify the accuracy of the simulation, we simulate an identical machine in a commercially available FEM package called *Ansys Maxwell*.

3.1.2 Ansys Maxwell

Compared to *SEMFEM*, *Maxwell* can be considered more user friendly. It follows the pattern of modern CAD software and provides the user with a visual, point-and-click interface, rather than a script-based interface. *Maxwell* offers an increased variety of functions, especially when used in conjunction with other products in the *Ansys* family [32].

We only use *Maxwell* to verify the accuracy of the *SEMFEM* simulation results. *Maxwell* will not be used in the optimisation process as *SEMFEM* offers a distinct advantage here in terms of computational speed.

Figure 3.2 compares the torque results of *Maxwell* and *SEMFEM* and gives us the confidence to use the faster *SEMFEM* package in the rest of the design process. The discrepancy between the results of these two packages can be due

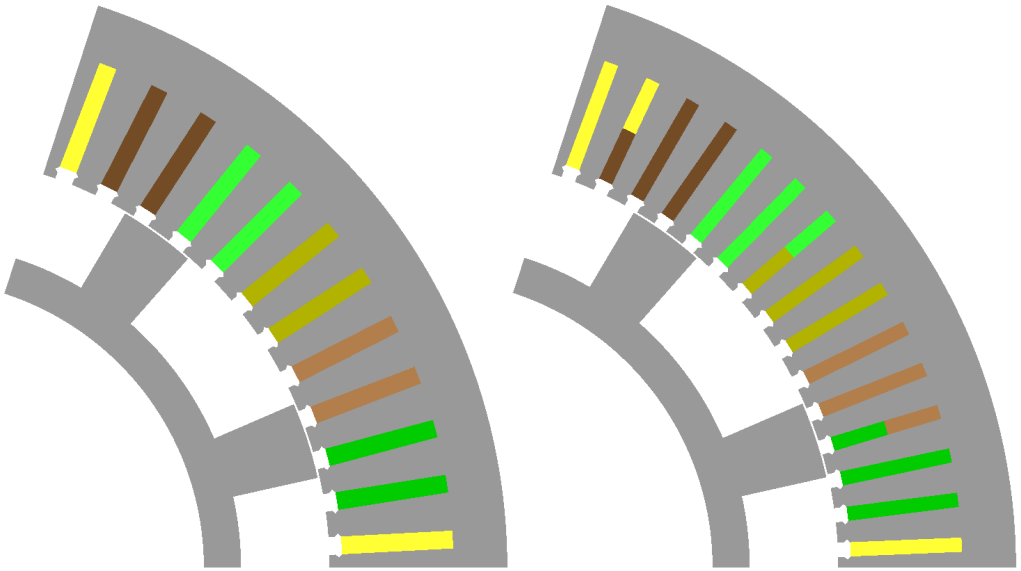

(a) (b)

Figure 3.1: Cross-sections of simple salient-pole 5 MW RSGs drawn in *SEMFEM*, with (a) an integral-slot (60 slots) winding and (b) a fractional-slot (75 slots) winding.

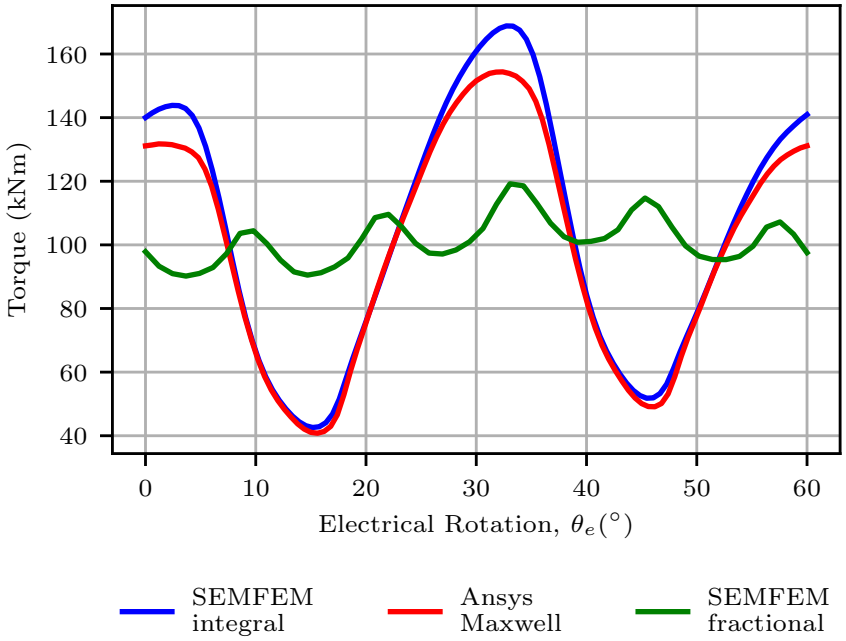

Figure 3.2: A comparison of two FEM packages simulating the RSG of Figure 3.1a, using an integral winding, and the RSG of Figure 3.1b, using a fractional-slot winding.

to a number of factors, but two of the most likely causes are the differences in the mesh structure, and differences in the the solver that is used. Before we consider the optimisation of the RSG, we will discuss two methods employed within *SEMFEM* in order to reduce the RSG's typically high torque ripple.

3.2 Torque ripple reduction

An inherent disadvantage of the RSM is a high torque ripple. The torque ripple percentage is calculated by,

$$T_{ripple} = \frac{T_{max} - T_{min}}{T_{avg}} \times 100, \tag{3.1}$$

where T_{max}, T_{min} and T_{avg} are the respective maximum, minimum and average torque values obtained from multiple FEM simulation rotor-steps. Various studies have been done in an attempt to reduce this phenomenon.

The well-cited work done by Bianchi et al. [33] showed that fractional-slot windings have the ability to reduce the torque ripple in synchronous machines. For a fractional-slot winding, the number of slots, per pole, per phase (designated as q) is a fraction. This serves to drastically decrease cogging between the stator teeth and the rotor poles.

Skewing is a design technique in which the rotor or stator is rotationally displaced along its stack length with a certain skew angle. This has proven to decrease the torque ripple of reluctance synchronous machines. Bomela and Kamper [34] showed that a conventional skew angle of one slot pitch decreases the torque ripple significantly - in their case to around 5%. Bomela's results show that there is little benefit in using more than 5 skewing stacks, or submachines, in the skewing simulation. Hubert et al. [35] argues that instead of continuously skewing, as little as two stacks can be used to drastically reduce torque ripple while minimizing the increase in manufacturing complexity that is typically brought about by skewing. Moghaddam's results [11] indicate that an increased skew angle generally results in a lower torque ripple. However, Bomela and Hubert show that the reduction in average torque, that is typically a result of skewing, is greater with an increase in the skew angle.

Asymmetry in RSMs has also been investigated for the purpose of torque ripple reduction. Sanada et al.[36] showed that an asymmetric flux barrier arrangement decreased the torque ripple of a RSM from around 50% to around 10% without a significant decrease in average torque. Moghaddam et al. [37] develops the ideas of Vagati et al. [38], to identify a single design parameter that could aid in the reduction of torque ripple when using asymmetric flux barriers. Howard et al. [17] also implements asymmetry as part of the optimisation procedure, along with significantly more complex flux barriers, and obtain similar torque ripple reduction results.

So, although asymmetry is shown to decrease torque ripple in RSMs, it is placed outside the scope of this study and the focus will remain on implementing skewing and a distributed fractional-slot winding.

3.2.1 Fractional-slot winding

Figure 3.1 shows two simple salient-pole machines with the only difference between them being their windings. RSG (a) has an integral winding, while RSG (b) uses a double-layered, overlapping distributed, fractional-slot winding. The winding is *fractional*, as the number of slots per pole, per phase, is equal to 2.5. The winding is *distributed* as each coil spans a number of slot-pitches and is distributed around the stator. The winding is *double-layered*, as every stator slot is filled with two winding coils - two layers of coils. Overlapping distributed windings are, as Spargo notes, "universally used in synchronous reluctance machines" [39].

The results in Table 3.1 serve to illustrate that 1) the simple salient-pole RSG has a very high torque ripple when using an integral winding, and 2) using a distributed fractional-slot winding dramatically decreases the torque ripple. This can also be seen in the earlier Figure 3.2, where the reduction in torque ripple due to a fractional-slot winding (shown in green) is contrasted with a RSG with an integral winding (shown in blue). Furthermore, the harmonics of the fractional-slot wound RSG in Figure 3.1b is shown in Figure 3.3. For this RSG, the winding factor is equal to 0.951, while for the RSG with an integral winding, the winding factor is 0.966 with the harmonics shown in Figure 3.4

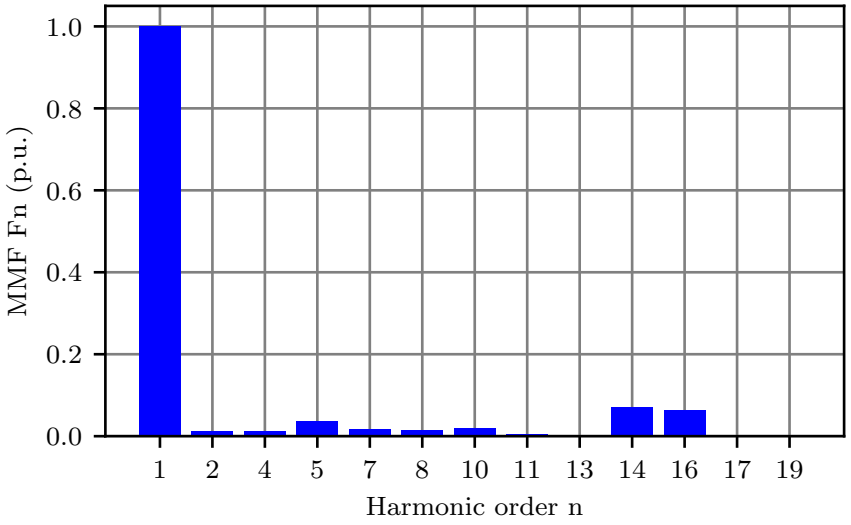

Figure 3.3: Harmonics of the fractional-slot wound RSG in Figure 3.1b

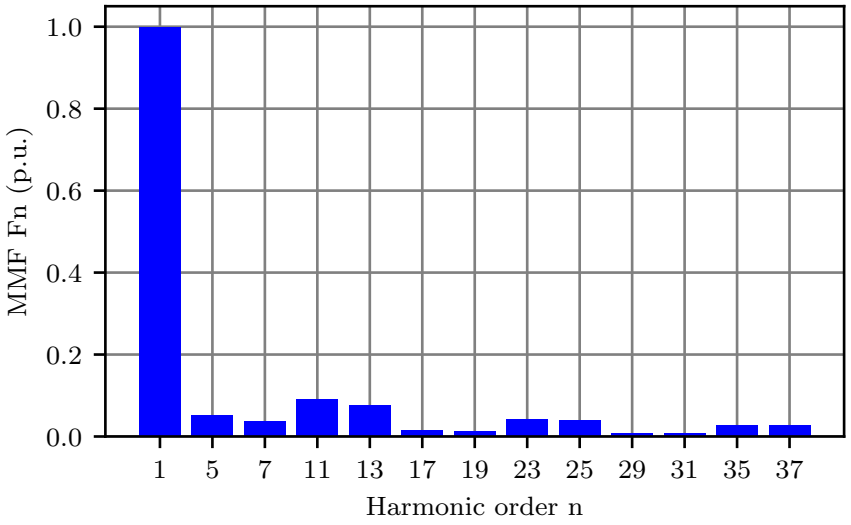

Figure 3.4: Harmonics of the integral-slot wound RSG in Figure 3.1a

Table 3.1: Torque ripple of unskewed salient-pole RSGs with different stator windings

Integral (Figure 3.1a)	Fractional (Figure 3.1b)
123.6 %	28.64 %

3.2.2 Rotor Skewing

To model a skewed machine in *SEMFEM*, the RSG is divided into five sub-machines. A *SEMFEM* simulation is a time-stepped simulation, so a single simulation has multiple steps. The five sub-machines are evaluated at each simulation step, from step 1 to step n. Each step represents the simulated machine after the passing of a certain amount of time. This also then corresponds with a certain rotational position, as the machine rotates over time.

Instead of simulating a single machine position at a single simulation step, when skewing is implemented, the average of the five sub-machines are associated with a single step. This is illustrated in Figure 3.5.

The final machine performance parameters are made up of the average of all these simulation steps, which are in turn made up of the average of the 5 sub-machine steps at a single position, as illustrated in Figure 3.6.

If the skew angle is a mechanical angle α, the positional rotation of the 5 sub-machines ($\alpha_{1\to5}$) are given by,

$$\begin{bmatrix}\alpha_1 & \alpha_2 & \alpha_3 & \alpha_4 & \alpha_5\end{bmatrix} = \begin{bmatrix}-2\frac{\alpha}{5} & -\frac{\alpha}{5} & 0 & \frac{\alpha}{5} & 2\frac{\alpha}{5}\end{bmatrix}. \tag{3.2}$$

The current angle of every sub-machine ($\theta_{1\to5}$) is also modified by adding the corresponding skew angle, converted to electrical degrees (α_e), to the optimum

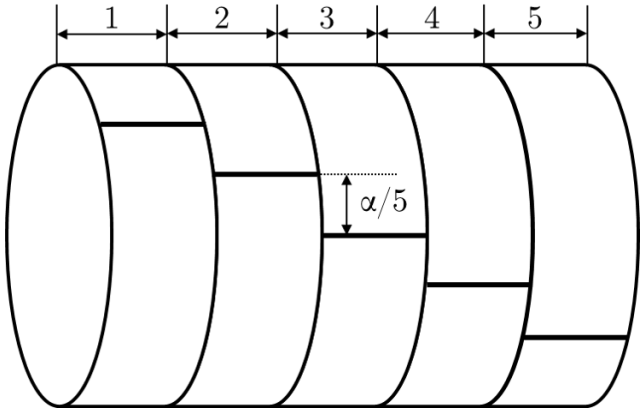

Figure 3.5: Skewing with 5 sub-machines at different positions, for a single simulation step.

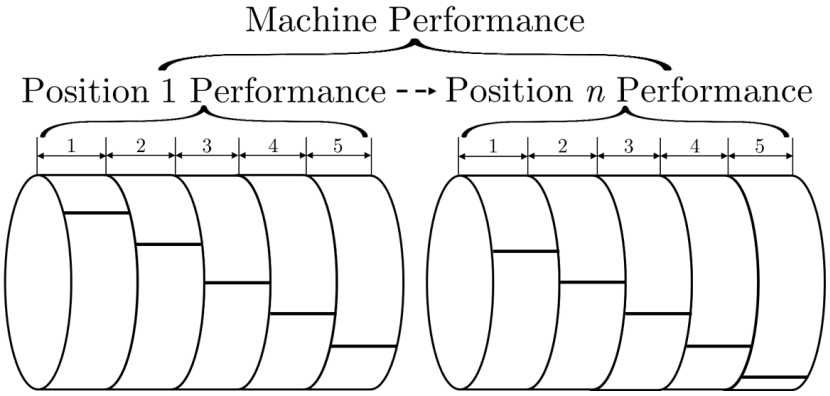

Figure 3.6: Machine performance determined from skewing simulation.

current angle (θ), as follows,

$$\begin{bmatrix}\theta+\alpha_{e1} & \theta+\alpha_{e2} & \theta+\alpha_{e3} & \theta+\alpha_{e4} & \theta+\alpha_{e5}\end{bmatrix}. \tag{3.3}$$

The 5-sub-machine skew simulation is repeated at a large enough number of different rotational positions, over 60 electrical degrees, to give accurate simulation results. Bomela and Kamper [34] note that no significant difference in simulation results is found with an increase in the number of sub-machines beyond 5. However, the specific skew angle used does have a marked impact on machine performance. The exact impact of skewing will be discussed in Chapter 6.

In this chapter, we have discussed how the RSG is verified with *Maxwell* and simulated in the faster *SEMFEM*, while including a distributed fractional-slot winding and skewing in the FEM simulation and calculation process. Skewing, combined with a fractional-slot winding is able to reduce the torque ripple of the RSGs investigated in this thesis to below 5%. We now look at the tools and processes used to optimise the RSG design.

Chapter 4

Optimisation

In the previous chapter we gave an overview of the FEM packages used in the simulation of the RSG, with specific focus on the package called *SEMFEM*. In this chapter, we will discuss how *SEMFEM* is used in conjunction with an optimisation package, called *VisualDoc*, in order to arrive at an optimum RSG design.

4.1 Connecting the optimisation and FEM packages

VisualDoc is an optimisation tool developed by Vanderplaats R&D [40]. It allows us to connect our *SEMFEM* simulation, that takes the form of a Python

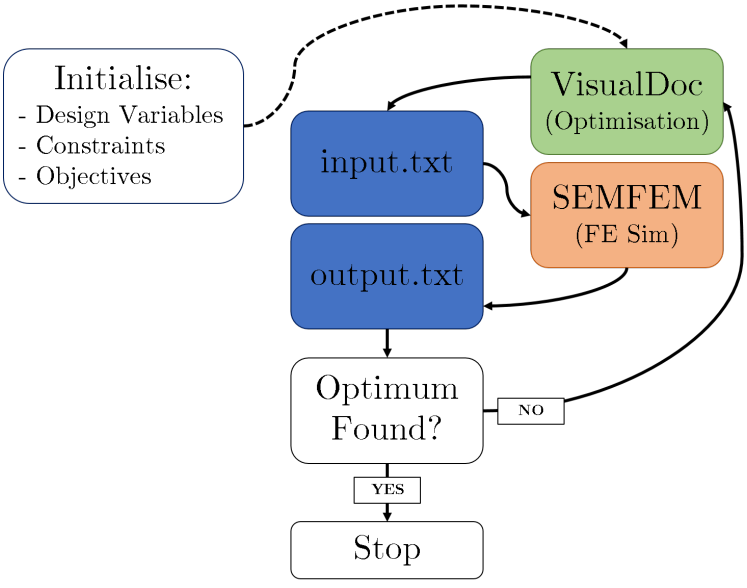

Figure 4.1: Optimisation Process using SEMFEM and VisualDoc.

script, with a multitude of optimisation algorithms. The optimisation process can be simply depicted as in Figure 4.1.

The first steps in using *VisualDoc* is to 1) input initial values for all the design variables, 2) specify any constraints that have to be met and 3) specify the optimisation objectives. After this initialisation process is completed, *VisualDoc* will start to iteratively change the design variables. These are the variables that are optimised by the optimisation algorithm and control the actual design of the RSG. These variables are saved in an *input.txt* file and serves as inputs to the *SEMFEM* Python file. They are used for every FE-simulation. The FE-simulation in turn produces an *output.txt* file that contains the performance parameters for the current iteration. These parameters are then used by *VisualDoc* as design objectives and constraints for that iteration. If the objectives are met, within the constraints and the solutions have converged, the optimisation will stop. If not, the process starts again with the design variables being slightly altered by *VisualDoc*.

VisualDoc recommends that the design variables are scaled, typically between -1 and 1, in accordance with their upper and lower design limits. They mention that "Optimization algorithms work best when the magnitudes of the constraint values are similar. This scaling brings the magnitude of the constraint values closer and helps the optimization algorithm in finding a solution." [41].

Such scaling can be done with,

$$x_i = \frac{z_i - (max([z_i]) + min([z_i]))/2}{(max([z_i]) - min([z_i]))}/2, \quad i = 1, ..., N. \tag{4.1}$$

Here, z_i are the un-scaled design variables, x_i are the resulting scaled variables used in the *VisualDoc* optimisation set-up and N is the total number of design variables in the optimisation process.

Between six and eight physical dimensions, encapsulating the rotor and stator, are used as design variables for the RSGs in this thesis. An additional design variable is allocated for the current angle, θ. The physical design variables for a representative simple salient-pole RSG can be seen in Figure 4.2.

4.2 Optimisation Strategy

The RSG is optimised using the multi-objective, non-dominant sorting genetic algorithm (NSGA-II). The optimisation consists only of a single objective; maximising the power factor:

$$F(X) = maximize\left[PF\right]. \tag{4.2}$$

This is subject to the following constraints:

$$G(X) = \begin{bmatrix} \eta & \geq 98\% \\ P_{out} & \approx 5MW \\ T_{ripple} & \leq 5\% \end{bmatrix}. \tag{4.3}$$

Gradient-based optimisation algorithms, like the Modified Method of Feasible Directions (MMFD) or Sequential Linear Programming (SLP) method, are much faster than the NSGA-II. However, gradient-based algorithms run the risk of falsely identifying a local optimum as a global optimum. A method that can be used to counteract the identification of false optima using *VisualDoc* is re-running a gradient-based optimisation, using various different initial values for the design variables. This will potentially force the algorithm to by-pass troublesome false optima and find a true, global optimum.

A method that has proven to increase the speed of optimisation, when using *VisualDoc*, is to manually combine a gradient-based algorithm, like MMFD or SLP, with NSGA-II. The idea is to observe the results of an initial NSGA-II optimisation and when the optimum results start to converge, the optimisation should be stopped prematurely. The current *optimum* values for each of the design variables can then be used as the *initial* values for those variables, but with a gradient based algorithm instead. It can take a long time for a plateaued

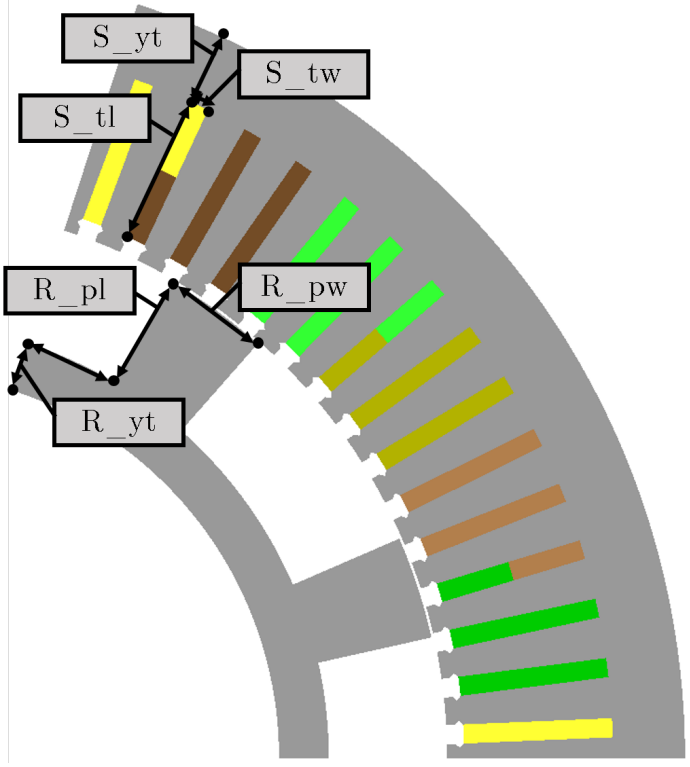

Figure 4.2: Illustration of the physical design variables for a simple salient-pole RSG optimisation.

NSGA-II optimisation to run its full course. Using a gradient-based algorithm as part of the process can decrease the time needed to achieve an optimum result.

It is also worth mentioning that a brief mesh independence study can help to further decrease optimisation time. The idea is to adjust the mesh for the FE-simulation iteratively in order to find an acceptable level of mesh density that provides reasonable accuracy, compared with a FE-simulation using a much denser mesh. The less dense the mesh is, the faster the FE-simulation (and hence the optimisation) will be.

Although there are minor changes, the basic optimisation process briefly described in this chapter is used in the following chapters as well. In the next chapter a series of optimum, simple salient-pole RSG designs is delivered using this optimisation method.

Chapter 5

Salient-pole RSG

In the previous chapters, we established the methods and tools that are used to arrive at an optimum RSG. In this chapter we apply this optimisation process to a simple salient-pole RSG. For this simple salient-pole structure, shown in Figure 5.1, we suggest a simplified torque equation that can be used to estimate sizing and get a quick idea of such an RSG's torque capability. As a further attempt to improve the quite low power factor of this RSG, we make a series

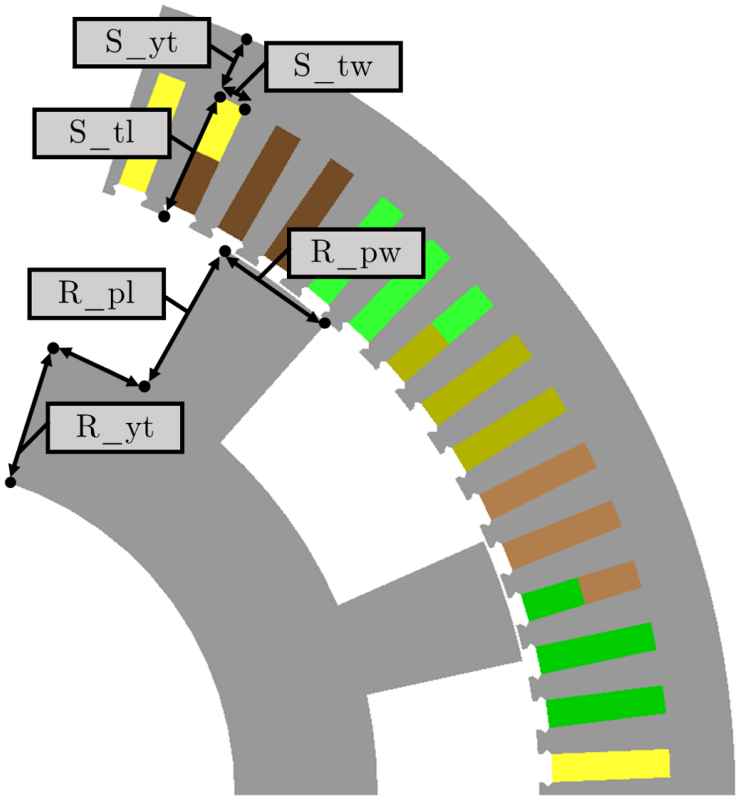

Figure 5.1: Optimisation structure and parameters of the simple salient-pole RSG.

of simple modifications to the simple salient-pole rotor, namely 1) tapering, 2) chamfering and 3) slitting. The rationale for the different design alterations is also discussed here. Finally, we compare the different optimum RSG designs and discuss the results.

5.1 Simple Salient-pole RSG

As mentioned in Chapter 1, one of the simplest rotor designs an RSG can have is a salient-pole type rotor. The simple salient-pole rotor structure shown in Figure 5.1 is denoted as *simple*, as it requires the lowest number of design variables to define its dimensions, of all the salient-pole RSG designs discussed in this thesis. It can therefore be used as a baseline to compare more complicated designs against. The simple salient-pole RSG is designed by optimising the design parameters illustrated in Figure 5.1.

A simple torque equation is developed for the specific machine structure of this RSG. The reason for this is to quickly verify the torque capability of the generator. Furthermore, the equation can be used for the initial sizing of such a generator.

5.1.1 Simplified torque equation

To derive a simple torque equation, a capture of the air-gap flux density of the RSG under full load is used, as shown in Figure 5.2. The averaged flux density waveform in Figure 5.2 is further simplified to that shown in Figure 5.3. With this simplification, the q-axis radial flux between the rotor poles is assumed to be zero.

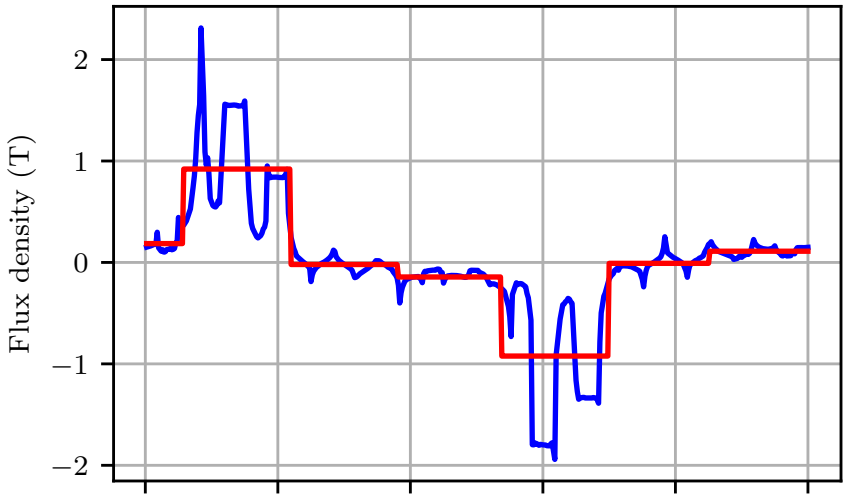

Figure 5.2: Capture of actual and averaged air-gap flux density waveforms of the RSG under full load.

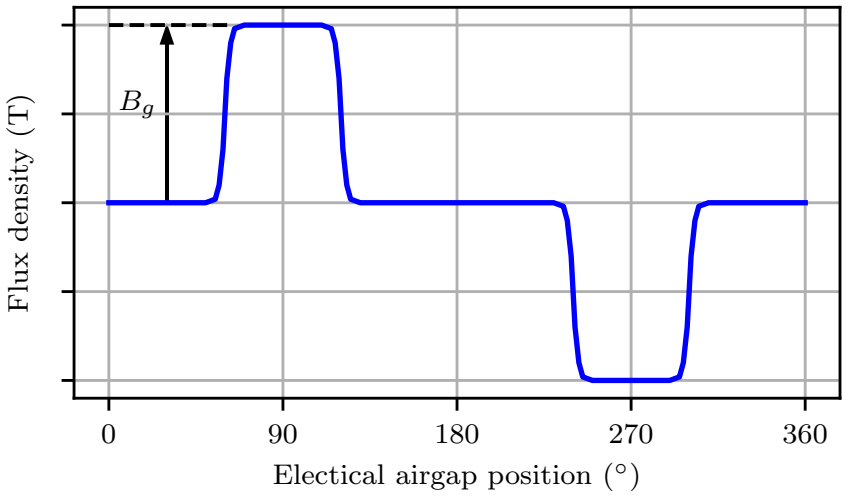

Figure 5.3: Assumed air-gap flux density waveform of the RSG.

In Figure 5.3, B_g is the average peak-plateau flux density in the air-gap between the rotor pole and the stator core teeth. This flux density can be determined from FE- or simple magnetic equivalent circuit analyses. Using the concept of the Lorenz force, a torque equation is derived similar to the torque derivation for brushed- and brushless DC machines. From the Lorenz force law the torque of the RSG can be expressed as

$$T_e = \frac{d_g}{2} B_g l_s I_{TP}, \tag{5.1}$$

where I_{TP} is the total current in the magnetic field. The total current in the magnetic field is the total q-axis current in the magnetic field and can be derived as

$$I_{TP} = \pi d_g k_r \sqrt{2} A_{rms} \sin\theta, \tag{5.2}$$

where θ is the current angle, $k_r = \theta_r/\theta_s$ and where θ_r is the mechanical rotor pole pitch and $\theta_p = 2\pi/p$ is the magnetic pole pitch. In (5.2) A_{rms} is the RMS current loading which is given by

$$A_{rms} = \frac{J_s A_{cu} k_f N_s k_A}{\pi d_g}, \tag{5.3}$$

where k_A is a correction factor for chorded and fractional-slot windings given by

$$k_A = \frac{N_{s1}}{N_s}\left(1 - \frac{\sqrt{3}}{2}\right) + \frac{\sqrt{3}}{2} \approx 0.134\frac{N_{s1}}{N_s} + 0.866. \tag{5.4}$$

In (5.3), N_{s1} is the number of those stator slots that have coil layers of the same phase. Replacing (5.2) and (5.3) into (5.1) and simplifying by assuming a current angle of $\theta = 45°$ we obtain

$$T_{e(2)} = \frac{1}{2} N_s B_g J_s A_{cu} k_f k_r k_A d_g l_s, \tag{5.5}$$

where N_s is the number of stator slots, k_r is an active slot factor and k_A a correction factor for chorded windings. Further in (5.5), J_s is the RMS stator current density, A_{cu} is the copper area of the slot, k_f is the stator slot fill factor, d_g is the air-gap diameter and l_s is the stack length of the core.

5.1.2 Performance of the simple salient-pole RSG

A summary of the performance results of the simple salient-pole RSG is shown in Table 5.1. The performance of the simple salient-pole RSG, before any modifications to the rotor, is already quite surprising. Using a distributed fractional-slot winding and skewing, which is explained in Chapter 3, a torque ripple of less than 5% is obtained. The impact of skewing will be further discussed in Chapter 6. In spite of a good torque density, efficiency and torque ripple, the power factor is quite low. This RSG is subsequently subjected to further minor modifications in an effort to improve the power factor.

Table 5.1: Performance summary of the simple salient-pole RSG

Parameter	Unit	Value
Power out	[MW]	5.023
Power factor		0.539
Efficiency	[%]	97.94
Torque average	[kNm]	97.94
Torque ripple	[%]	4.74

5.2 Modifications to the Rotor

The rotor of the simple salient-pole RSG is modified and optimised with the same procedure described in Chapter 4. The goal is to maximise the power factor while aiming for a torque ripple of 5%, an efficiency of 98% and a power output of 5 MW. The design variables that determine the physical dimensions of the RSGs are explained in Section 5.3, in Table 5.2. The performance results of the optimised modified RSGs are in displayed in Table 5.3 also as part of Section 5.3. An optimisation is done for each of the three following rotor modifications: tapering, chamfering and slitting.

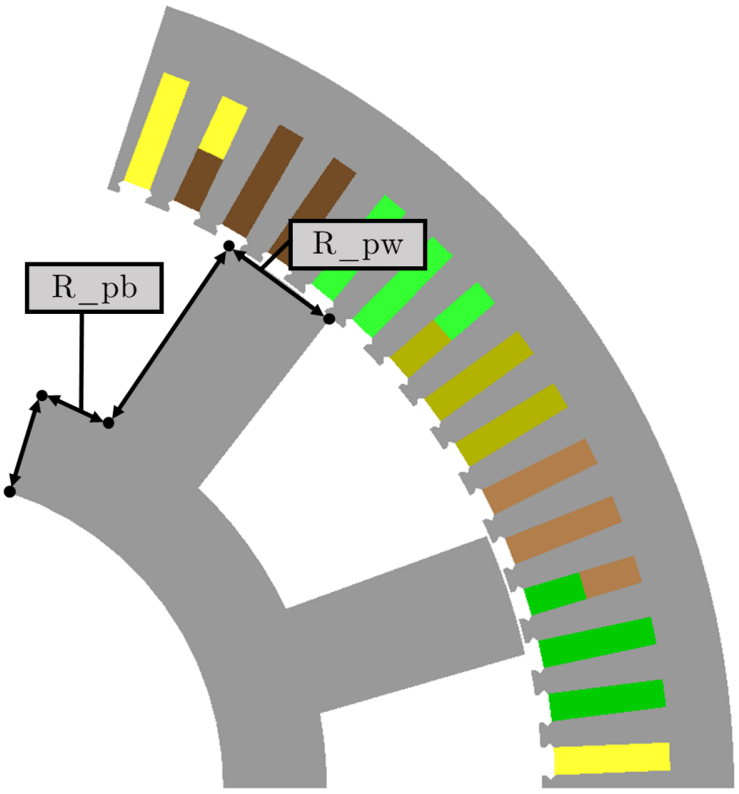

Figure 5.4: Optimisation structure and parameters of the tapered RSG.

5.2.1 Tapered RSG

A rotor with tapered poles can be found in other non-permanent magnet rotors, such as the SRM of Ptakh et al. [42] or the WF-FSG of Akuru and Kamper [43]. This rotor topology and its distinguishing optimisation parameters are illustrated in Figure 5.4. The significant difference between the tapered RSG and the simple salient-pole RSG is an additional parameter that enables the pole to taper by increasing or decreasing dimension *R_pb*. This means that dimension *R_pl* would typically not be in line, radially, with the shaft center point, while the *R_pl* dimension of the simple salient-pole RSG always proceeds radially from the shaft center. It was found that this rotor design slightly improved the power factor without negatively impacting other performance parameters.

5.2.2 Chamfered RSG

Rakgati et el. [44] found that chamfering the rotor poles of their multi-phase reluctance machine yields a slight improvement in performance. This is put to the test in a design optimisation with distinguishing optimisation variables, as in Figure 5.5a, allowing a type of chamfering to take place. The optimisation tends to make the chamfer quite large by increasing *R_cl*. In effect, the

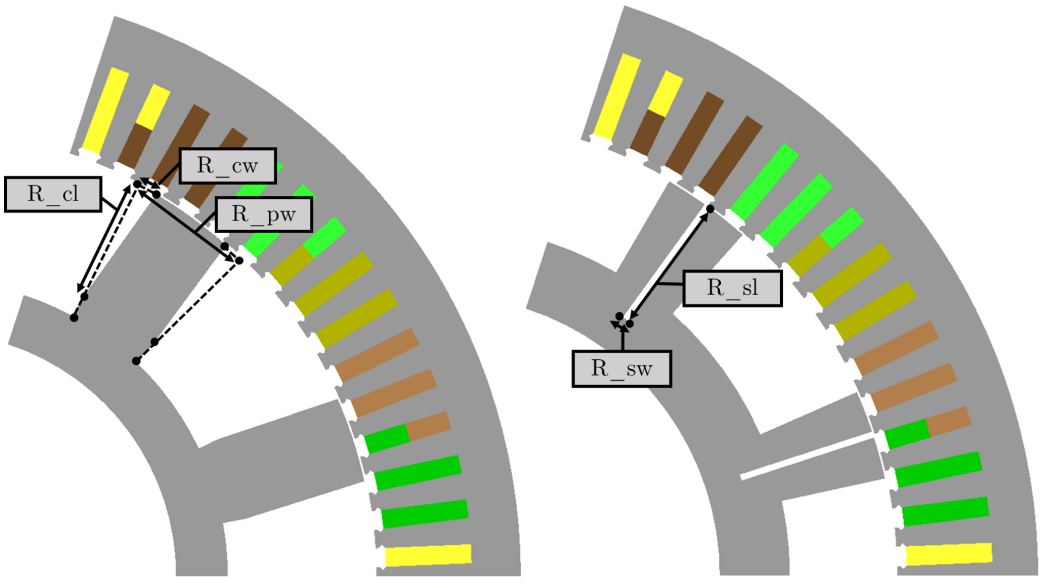

(a) (b)

Figure 5.5: Optimisation structure and parameters of (a) the chamfered RSG and (b) the slitted RSG.

chamfered RSG resembles the tapered RSG.

When the chamfering is much more constrained in an attempt to force the optimisation into a design that resembles that of Rakgati, the optimum machine tends to have little, to no chamfering present. This indicates that the chamfering has little effect on the salient-pole RSG performance. Although the chamfered RSG in Figure 5.5a (resembling the tapered RSG) shows slight improvement over the simple salient-pole RSG, it does not show more improvement than the tapered RSG. A further attempt to chamfer only one side of the rotor pole, in order to potentially benefit from asymmetry, also does not result in any improvement.

5.2.3 Slitted RSG

Rakgati et al. also found that adding *slits* in the rotor pole of their multi-phase reluctance machine yields a slight improvement in performance [44]. The idea is that slitting minimizes the q-axis flux and thus improve the saliency ratio and overall machine performance. Figure 5.5b shows the distinguishing design parameters for this rotor topology.

It is telling that the optimisation consistently attempts to decrease the slit size, by decreasing R_sw, until the slit becomes insignificantly small. When the slit size is constrained in order to keep it from being too small, the slitted RSG's performance did not improve compared to the other salient-pole RSGs. This was tested for an optimisation with a single slit, as in Figure 5.5b, as well

as an optimisation with two variably spaced slits in the rotor pole.

Before we compare and discuss the performance of the various salient-pole RSG's, we discuss the derivation of a simplified torque equation for the salient-pole type RSG.

5.3 Optimum Design Assessment and Comparison

The optimum dimensions of the four RSGs are given and explained in Table 5.2. Of these dimensions, the air-gap diameter, but more particularly the rotor pole arc, are of interest. For all the RSGs, an optimum rotor pole arc of approximately 57° electrical is found. This is important information for the design engineer at initial design.

Based on the optimum performance results of Table 5.3, the tapered salient-pole RSG is the design choice that shows the most significant improvement compared to the simple salient-pole RSG. Although this improvement is not exceedingly significant, tapering seems to be an adaptation worth adopting when designing a salient-pole RSG, as it will be similar to the simple salient-pole RSG in terms of manufacturing and mechanical strength.

The performance of the tapered salient-pole RSG versus current angle is displayed in Figure 5.6. As is shown, a current angle of 54.34° at full load gives the best compromise for good torque, power factor and efficiency, while still maintaining a torque ripple lower than 5 %. The performance of this RSG is further compared, in Table 5.4, with that of the classical flux-barrier

Table 5.2: Optimised dimensions of the salient-pole RSGs

Var	Description	Simple [mm]	Taper [mm]	Chamfer [mm]	Slit [mm]
S_yt	Stator yoke thickness	74.06	73.43	79.03	72.10
S_tw	Stator tooth width	16.06	16.01	15.15	15.37
S_tl	Stator tooth length	149.5	147.7	152.9	150.3
R_yt	Rotor yoke thickness	163	119.1	83	110.7
R_pw	Rotor pole width	143.4	143	188.8	143.4
R_pl	Rotor pole length	181.4	244.5	235.8	277
R_pb	Rotor pole base	115.1	86.3	86	118.7
R_sw	Rotor slit width	-	-	-	9.97
R_sl	Rotor slit length	-	-	-	219.5
R_cw	Rotor chamfer width	-	-	24.97	-
R_cl	Rotor chamfer length	-	-	200.6	-
R_ir	Rotor inner radius	374	357.2	391.3	442.6
R_or	Rotor outer radius	718.50	720.8	710.1	719.6

Table 5.3: Performance summary and comparison of salient-pole RSGs

Parameter	Unit	Simple	Taper	Chamfer	Slit
Power out	[MW]	5.023	5.01	5.02	4.88
Power factor		0.539	0.543	0.541	0.538
Efficiency	[%]	97.94	97.90	97.87	97.86
Torque average	[kNm]	97.94	97.67	98.02	95.22
Torque ripple	[%]	4.74	4.82	4.88	5.62

rotor, synchronous reluctance wind generator of Howard [7]. As mentioned in Chapter 1, Howard's RSG serves as a published equivalent flux-barrier RSG that is used for comparison with the simpler RSGs throughout this thesis.

It is worth noting that the tapered salient-pole RSG offers a similar torque density to this distributed flux-barrier rotor RSG, with an equivalent volume. The main difference is the much lower power factor, as expected of the tapered salient-pole rotor RSG. The developed torque calculated according to the analytical torque equation (5.5) is also given in Table 5.4, as $T_{e(2)}$, for the tapered RSG. This predicts a slightly too high torque as expected, but is reasonably

Table 5.4: Comparison of Howard's RSGs with the tapered salient-pole RSG in Figure 5.4

Parameter	Unit	RSG of [7]	Tapered RSG
Power out	[MW]	5.05	5.01
Torque average	[kNm]	98.4	97.67
Torque $T_{e(2)}$	[kNm]	-	108
Efficiency	[%]	98.0	97.90
Power factor		0.853	0.543
Torque ripple	[%]	-	4.82
Poles		10	10
Slots per pole		9	7.5
Fill factor		0.35	0.6
Stator diameter	[m]	1.89	1.89
Stack length	[m]	1.88	1.89
Air-gap	[mm]	2.5	3
Torque density	[kNm/m^3]	18.65	18.42
Current angle	[°]	73.4	54.34
Current density	[A/mm^2]	4.5	2
Speed	[r/min]	500	500
L_d	[mH]	-	151.6
L_q	[mH]	-	39.78
L_d/L_q	[mH]	-	3.81

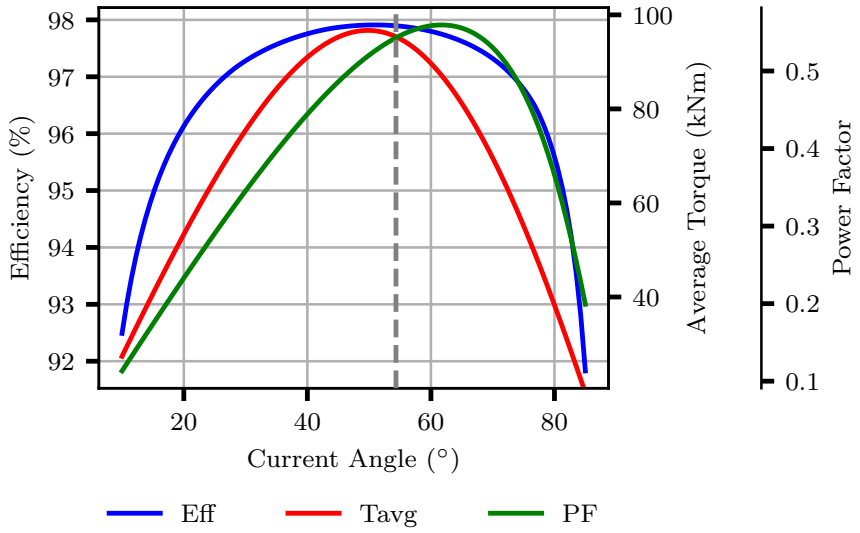

Figure 5.6: Performance of the tapered salient-pole RSG in Figure 5.4

close for a first estimation and provides confirmation of the torque capability of the salient-pole RSG.

The low power factor increases the MVA capability and cost of only the synchronous rectifier side of the power electronic converter (not the grid-tie inverter side). However, the very cheap proposed salient rotor of the RSG potentially compensates for this increased cost. In fact, Boldea et al. [45] recently investigated a 10 MW, directly driven, synchronous reluctance wind generator which has a power factor below 0.5. Their study suggests that the higher converter costs may be compensated for by the RSG's higher efficiency and lower initial active system set-up costs.

Yet, in an attempt to further increase the low power factor, the next chapter presents a "split-pole" RSG. It develops the idea behind the slitted RSG by fully splitting the salient rotor-pole, resulting in an increased saliency ratio and an improved power factor.

Chapter 6

Split-pole RSG

In the previous chapter we present a synchronous reluctance wind generator with a salient-pole rotor. The design parameters are kept as close as possible to the distributed flux barrier RSG of Howard [7], [14], allowing us to effectively compare the performance of the designs. The greatest difference between the RSG of Howard and the simple salient-pole RSG is the power factor. The salient-pole RSG has a low power factor of around 0.54. In an effort to increase this low power factor, a split-pole RSG is presented.

6.1 Design and Optimisation

The optimisation of the simple salient-pole RSG in Chapter 5 resulted in a range of different salient-pole RSG designs that were very similar in performance and can all be considered optimum designs. One of those optimum designs is the RSG shown in Figure 6.1a. This will be compared to the split-pole RSG, displayed in Figure 6.1b, in this chapter.

The aim of the split-pole RSG is to increase the power factor, by increasing the saliency ratio (L_d/L_q). The slit in the middle of the rotor pole serves to decrease the q-axis flux linkage and increase the d-axis flux linkage. This correlates directly to the q-axis and d-axis inductances and thus influences the saliency ratio.

The optimisation design variables for the physical dimensions of the split-pole RSG is shown in Figure 6.2a, with the dimensions given in Table 6.1. A similar design process is followed as for the salient-pole RSG of Chapter 5. Once again, skewing and a distributed fractional slot winding is used to limit the torque ripple to 5%. This time, the optimal skew angle is also investigated.

6.1.1 Optimal Skew Angle

It is established that the RSGs in Figure 6.1 require skewing to decrease the torque ripple to below 5%. A distributed fractional-slot winding on its own is

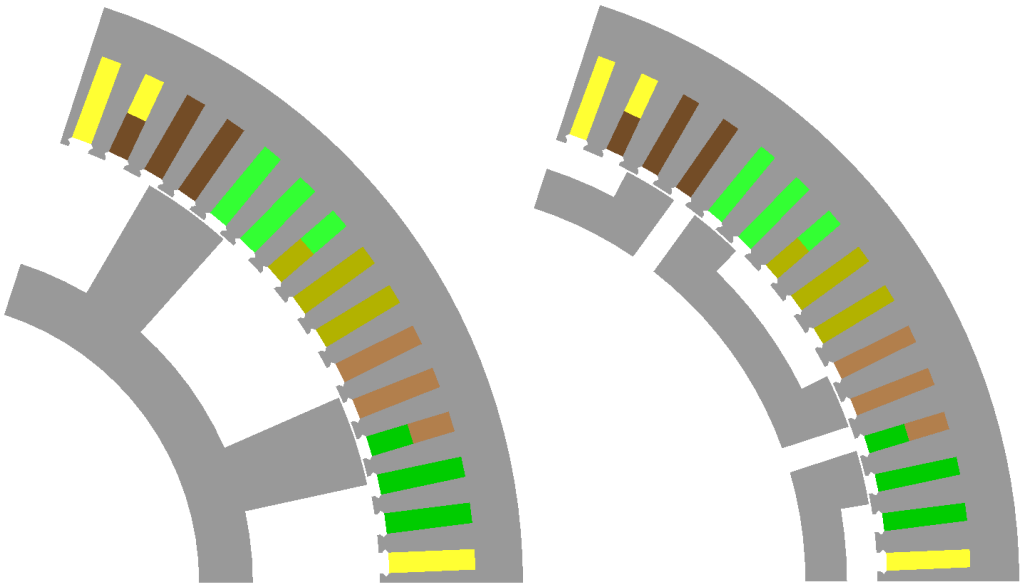

(a) (b)

Figure 6.1: RSG cross-sections showing (a) the simple salient-pole RSG and (b) the split-pole RSG.

not sufficient. The question is then, what is the best skew angle for optimum machine performance? To answer this question, the skew angle is included as an additional design variable, as part of an initial optimal skew angle investigation. This initial investigation shows that a skew angles close to one- and two slot-pitches give the best results. More focused optimisations are then performed on split-pole RSGs with a skew angle of one- and two slot-pitches respectively.

It is interesting to note that both these skew angles result in two physically different machines, shown in Figure 6.2. They do, however, have similar per-

Table 6.1: Optimised Dimensions of the salient-pole and split-pole RSGs

Dimension	Description	Salient Pole [mm]	Split-Pole [mm]
S_yt	Stator yoke thickness	74.1	75.99
S_tw	Stator tooth width	16.07	14.07
S_tl	Stator tooth length	149.46	145.11
R_yt	Rotor yoke thickness	83.8	64.71
R_pw	Rotor pole width	143.32	210.75
R_pl	Rotor pole length	194.7	44.19
R_gw	Rotor gap width	-	39.45
R_ir	Rotor inner radius	439.9	612
R_or	Rotor outer radius	718	720.90

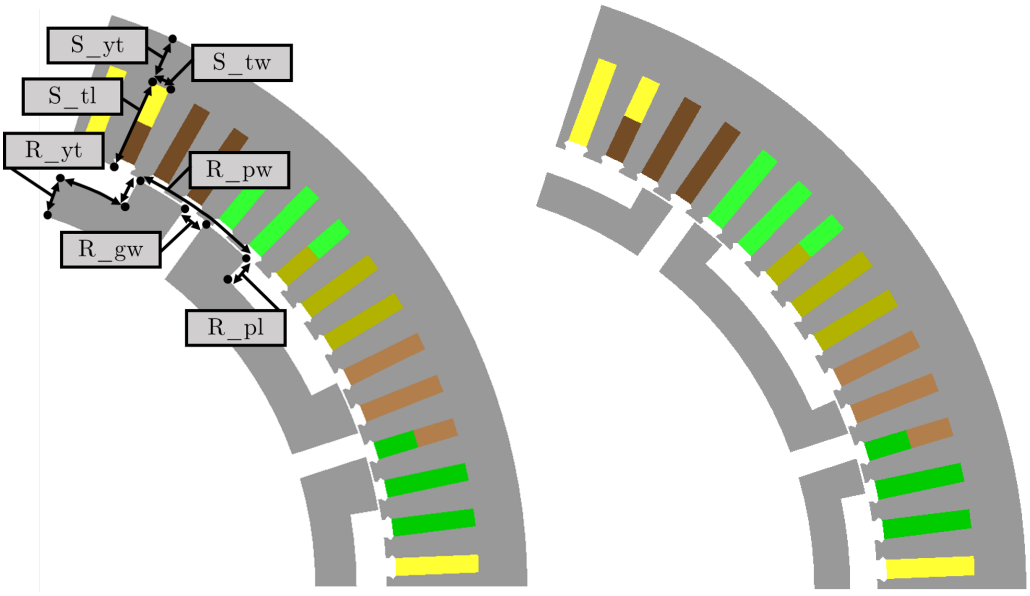

(a) (b)

Figure 6.2: Optimised split-pole RSG cross-sections of (a) the 2 slot-pitch skewed RSG, showing design variables, and (b) the 1 slot-pitch skewed RSG.

formance parameters, as seen in Table 6.2. From this results, it can be seen that the two slot-pitch skewed RSG fares slightly better. Although a skew angle of 1 slot-pitch is framed as conventional by Wang et al. [46] and Bomela [34], the optimisation results concur with Hubert et al. [35] and Howard [17] in that 1 slot-pitch is not necessarily the optimal skew angle. In a design optimisation where skewing is implemented to decrease the torque ripple, it would be prudent to investigate which skewing angle is best for a specific design that has a specific torque ripple requirement.

Furthermore, it was found that care should be taken when selecting a skew angle, as rapid fluctuations in torque can go undetected if too few simulation steps are used. Too few steps would give a seemingly lower, but inaccurate, torque ripple result.

Table 6.2: Design optimisation results of the individually optimised, 1- and 2 slot-pitch (SP) skewed, split-pole RSGs of Figure 6.2

	Unit	2 SP Skewed	1 SP Skewed
Pout	MW	5.030	5.007
Torque average	kNm	97.87	97.32
Torque ripple	%	4.82	5.02
Power factor		0.649	0.648
Efficiency	%	98.15	98.27

Finally, Moghaddam [11] and Hubert [35] show that the torque ripple of RSMs generally decrease with an increase in skew angle. It is also adversely shown that an increase in skew angle corresponds to a decrease in the average torque. This is evident from Figure 6.3, for the split-pole RSG of Figure 6.1b. Figure 6.3 shows that although a skewing angle of two slot-pitches (shown in red) offers a lower torque ripple, it also has a lower averaged torque associated with it. A higher average torque is obtained with a single slot-pitch skew angle (shown in green), but with a greater torque ripple.

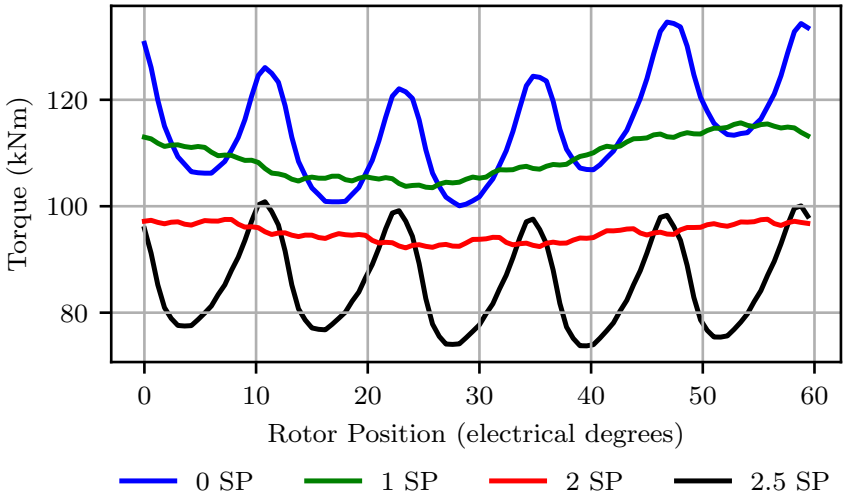

Figure 6.3: Instantaneous torque versus rotor position of the split-pole RSG of Figure 6.1b with skew angles in terms of slot-pitches (SP) as a parameter.

6.1.2 Performance Comparison

The performance of the optimised split-pole RSG can be seen in Figure 6.4. It is also compared in Table 6.3 with the salient-pole RSG and the RSG of [7]. It is worth noting that the salient-pole RSG has about 48% more active mass than that of Howard. The Split pole RSG reduces that to about 31% more active mass. The split-pole RSG also obtained similar torque densities to that of Howard with an equivalent volume and a similar efficiency.

The significant effect of the rotor pole gap on the flux linkages, and hence inductances, of the split-pole RSG compared to the salient-pole RSG, is evident from an increase in saliency ratio of 35%. An increase in the saliency ratio is well known to roughly correlate to an increase in power factor. More specifically, Tahi et al. [47] and Stipetic et al. [48] both show how power factor depends on a combination of current angle and saliency ratio. The power

factor is given by Stipetic et al. as

$$PF = \cos\phi = \frac{\xi - 1}{\sqrt{\xi^2 \frac{1}{\sin^2\theta} + \frac{1}{\cos^2\theta}}}, \tag{6.1}$$

where ϕ is the power factor angle, θ is the current angle and ξ is the saliency ratio. From this, Stipetic et. al then represents the maximum power factor with

$$\cos\phi_{max} = \frac{\xi - 1}{\xi + 1}. \tag{6.2}$$

It is clear from Equation (6.2) that an increase in saliency ratio roughly correlates to an increase in power factor.

Including split-poles in the design optimisation has the effect of increasing the power factor of the salient-pole RSG by about 20%. It notably increased the d-axis inductance by about 50%. Although a power factor of 0.65 for the split-pole RSG is a definite improvement on the salient-pole RSG's power factor of 0.54, it is still some way below the power factor of 0.853 obtained by Howard. The low power factor will, as mentioned before, increase the cost of only the synchronous rectifier side of the power electronic converter. This cost might be offset by a simpler manufacturing process and increased robustness. However, the split-pole design presents a challenge for the physical manufacturing of the rotor and is investigated in the next section.

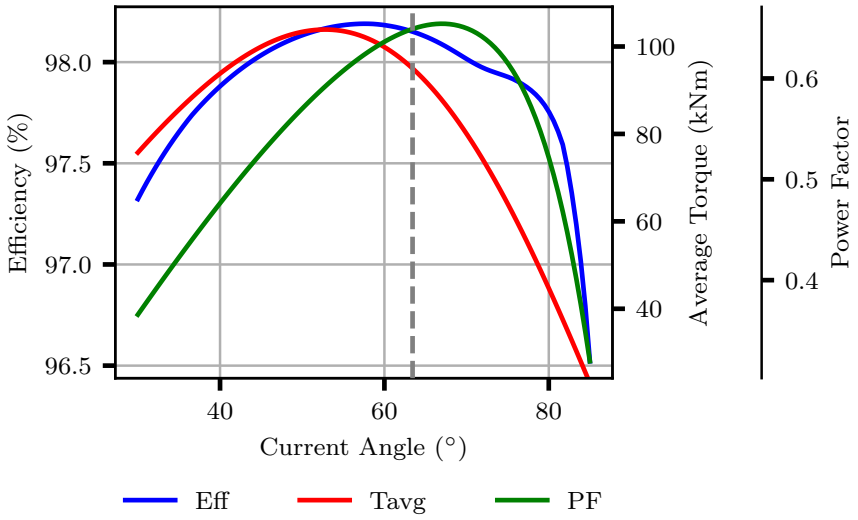

Figure 6.4: Performance versus current angle of the optimised split-pole RSG of Figure 6.1b.

Table 6.3: Comparison of Howard's distributed flux-barrier RSG, to those in Figure 6.1a and Figure 6.1b.

	Unit	RSG of [7]	Salient-Pole	Split-Pole
Power out	[MW]	5.05	5.00	5.03
Torque average	[kNm]	98.4	97.57	97.87
Efficiency	[%]	98.0	97.94	98.15
Power factor		0.853	0.539	0.649
Torque Ripple	[%]	-	4.92	4.82
Poles		10	10	10
Slots per pole		9	7.5	7.5
Fill Factor		0.35	0.6	0.6
Stator diameter	[m]	1.89	1.89	1.89
Stack length	[m]	1.88	1.88	1.88
Air-gap	[mm]	2.5	3	3
Torque density	[kNm/m^3]	18.65	18.50	18.56
Current angle	[°]	73.4	54.620	63.426
Current density	A/mm^2	4.5	1.414	1.414
Speed	[r/min]	500	500	500
L_d	[mH]	-	148.05	222.85
L_q	[mH]	-	39.62	44.07
L_d/L_q		-	3.74	5.06
Active Mass	[t]	14.8	21.97	19.42

6.2 Physical construction

The split-pole RSG has a rotor yoke that is situated quite far from the axis of the machine. For large machines of this nature, a spoked-arm rotor construction can be considered, as suggested by Sethuraman et al. [15]. In their work on the 10 MW DTU reference turbine, drawing from structural analysis done by McDonald [49], they use spoke-arms for their permanent magnet synchronous generator (PMSG) and electrically excited synchronous generator (EESG) designs.

However, for the split-pole RSG, every second pole should not be connected to a spoked-arm, if iron is used. Otherwise the magnetic field would travel along the spoke and defeat the purpose of the split-pole. This will result in 'floating poles' - rotor segments that are not directly connected to the shaft via a spoke-arm - which can be challenging to manufacture.

6.2.1 Manufacturing suggestions

A suggested manufacturing solution can be seen in Figure 6.5, where every second floating pole is keyed to a spoked pole on either side, using a cylindrical

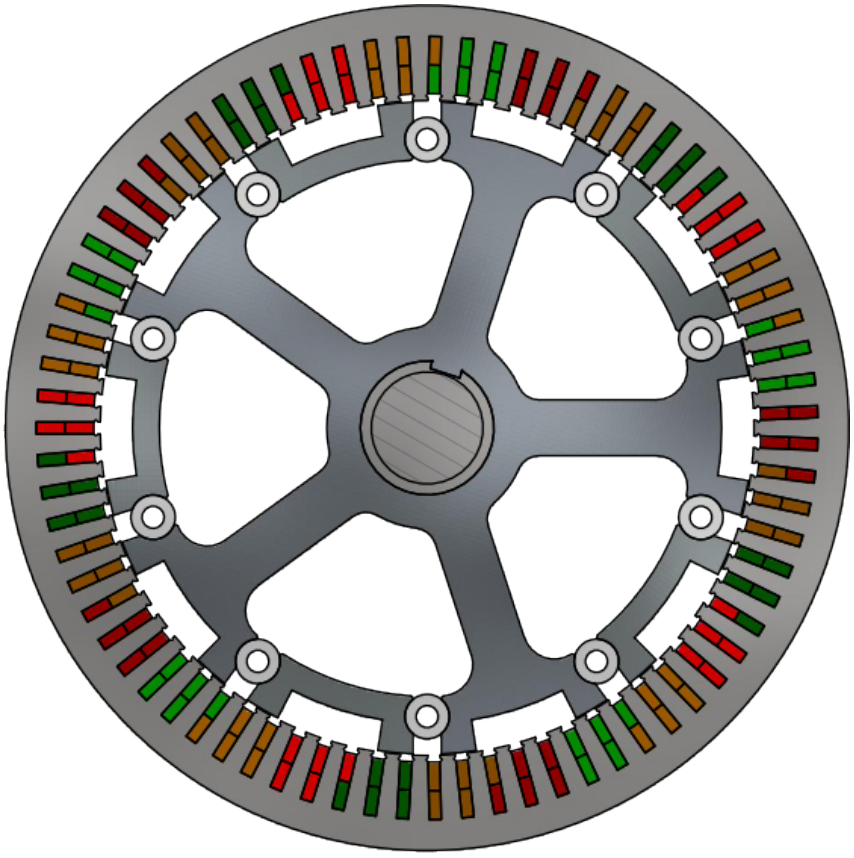

Figure 6.5: Suggested split-pole RSG with spoke-arms.

key. This split-pole RSG is a skewed machine with five sub-machine stacks. To assemble a skewed machine, each of the five sub-machine stacks has to be stacked and keyed, before moving on to the next relatively displaced stack.

For a spoked RSG, the effects of the spokes need to be taken into consideration. As can be seen in Figure 6.6, the flux lines do not travel along the

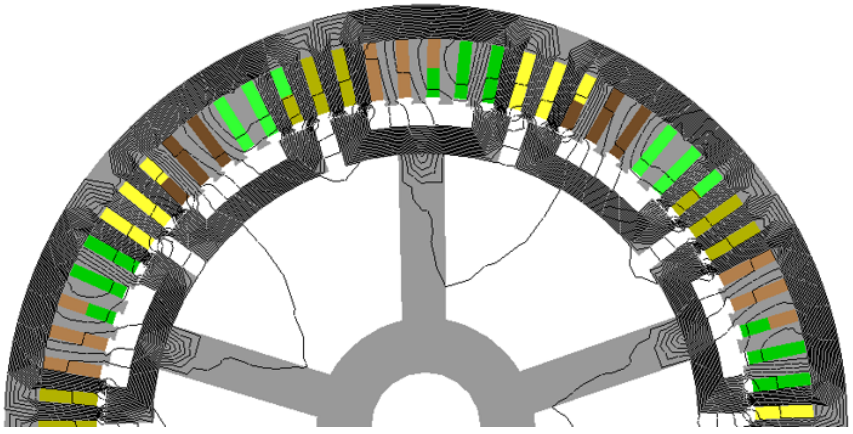

Figure 6.6: Flux lines showing the flux leakage for the split-pole RSG.

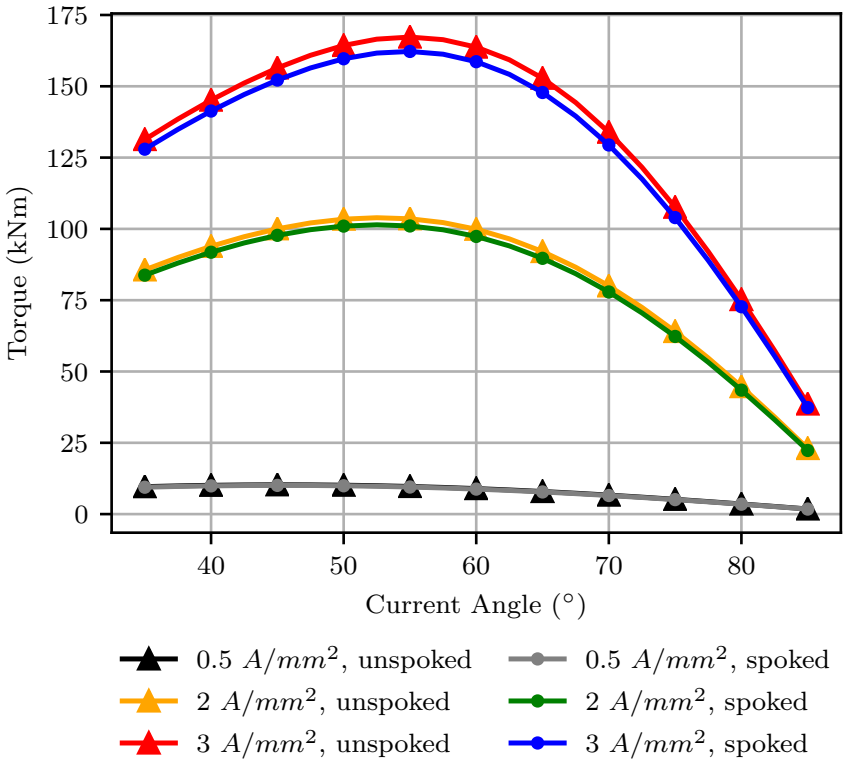

Figure 6.7: The effect of different current densities on the average torque versus current angle of the spoked and unspoked split-pole RSGs.

spokes in a significant way. However, the simulated results show a decrease in power factor of 3.6% due to increased leakage. As seen in Figure 6.7, the effect is slightly larger at higher current densities and higher average torque, which suits the wind generator application as wind turbines operate at partial loading for large portions of time.

Another manufacturing consideration could involve the magnetic isolation of the poles from the spokes, using non-magnetic material. In this case, every pole could have a spoke, instead of having floating poles and keys. The flux would then not be able to travel along the spokes, due to the non-magnetic nature of the spokes. To manufacture such a design, spokes would have to be fitted onto both the poles and the shaft. To assemble a skewed machine, the spoked poles can be fixed to the shaft at skewed shaft-spoke connection points. Alternatively, the spokes can be fixed to the shaft linearly, with the spokes being angled towards the top pole-side so that the poles are in the appropriate skewed position.

A final alternative method could involve the use of additive manufacturing as described by Wrobel and Mecrow [50]. However, it is currently and immature technology and the feasibility of such a design requires further research.

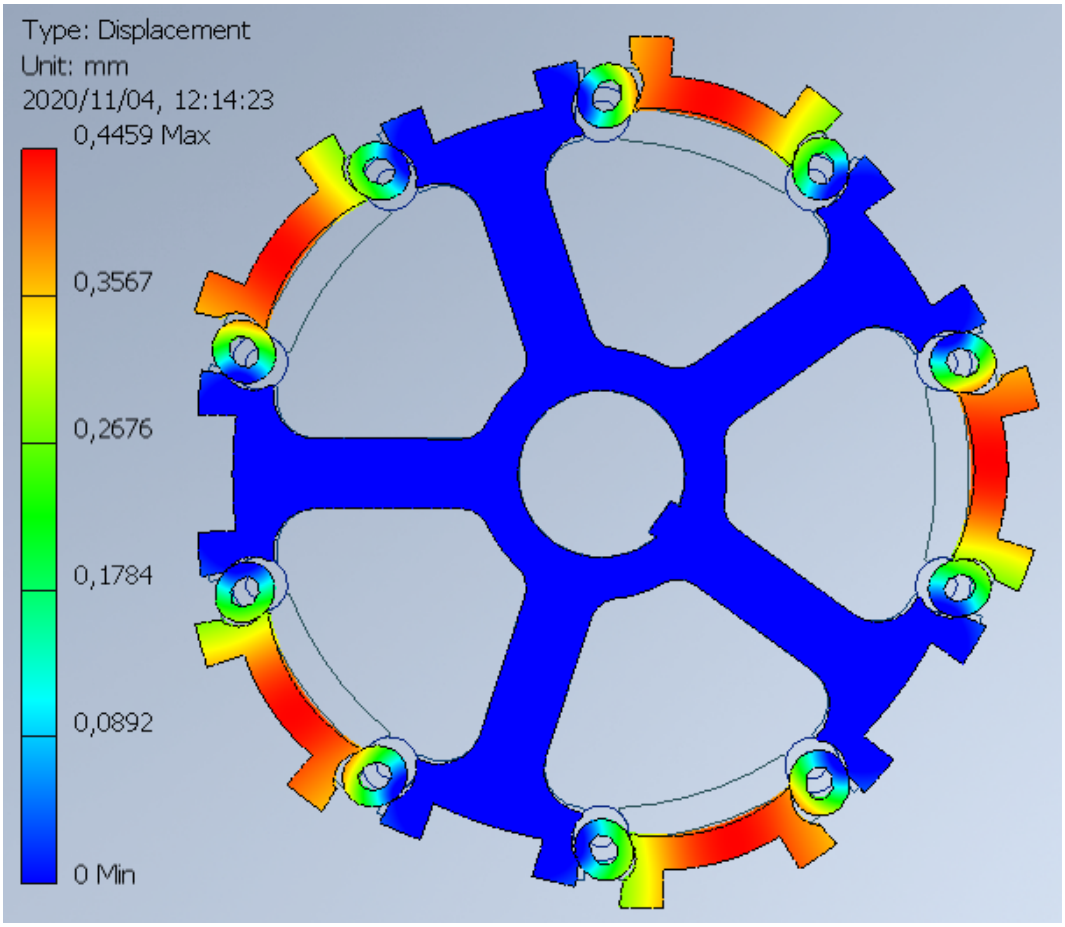

Figure 6.8: Deformation of initial split-pole RSG design.

6.2.2 Deformation and stress analysis

To determine whether the split-pole RSG using floating poles, spokes and keys would be a functional design, a structural analysis is done. For this purpose, the RSG is recreated in *Autodesk Inventor* [51]. From the *Environments* tab in *Inventor*, what is called a "Stress Analysis" is selected. A full-body "load" is applied to the rotor by causing it to rotate around its axis at 500 r/min. By assigning materials to the parts in the rotor assembly, inventor determines the mass of the parts and can therefore use the assigned angular velocity to determine the forces and related deformation of the assembly using a FE-simulation.

It should be noted that a thorough mechanical analysis falls outside the scope of this study. This section aims to take a step towards proving the feasibility of this construction method and make some basic recommendations based on the deformation results.

From Figure 6.8 it is clear that the split-pole RSG construction is functional. The maximum deformation is about 0.45 mm and occurs at the float-

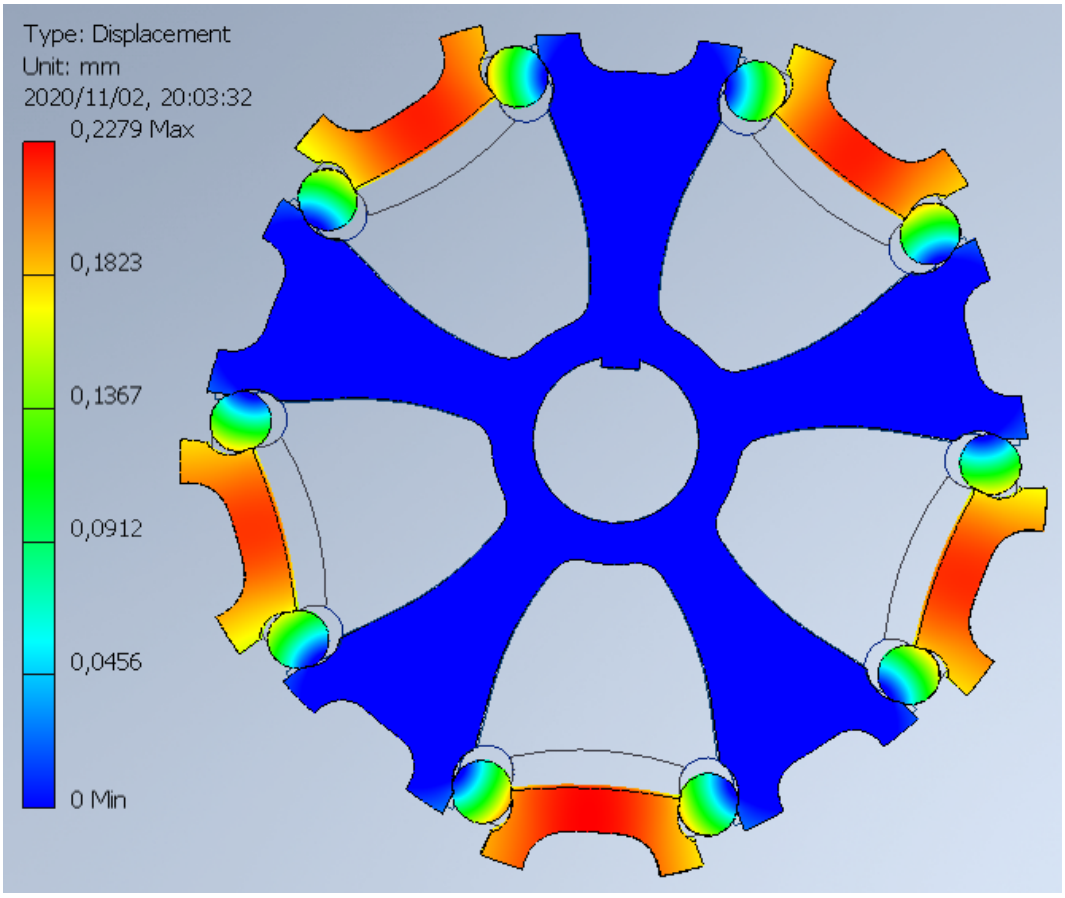

Figure 6.9: Decreased deformation after modifications to the initial split-pole RSG design.

ing poles, as expected. Although this initial deformation analysis confirms that the RSG will hold together, a few methods are suggested to decrease the deformation further.

1. Use solid cylindrical keys instead of hollow ones.
2. Change the curvature of the rotor pole segments in order to better resist the centrifugal force.
3. Reinforce the spoked poles at the pole-spoke connection points.

The results of applying these modifications are shown in Figure 6.9. The maximum deformation is decreased by about 49% to a value of around 0.23 mm.

In conclusion, this chapter presents the split-pole RSG and shows that splitting the poles of the simple salient-pole RSG increases it's power factor by about 20%. The cost of a better power factor is increased manufacturing

complexity. A potential solution to the challenge of manufacturing the split-pole design is presented. A simple deformation analysis is completed and should be verified with more rigorous simulations, however, this falls outside the scope of this study. The results of a simple stress-analysis of the machines in Figure 6.8 and Figure 6.9 is shown in Appendix A.

Chapter 7

Conclusions and Recommendations

7.1 Conclusions

Literature concerning multi-megawatt reluctance synchronous machines is quite scarce. This is even more true when the focus shifts to multi-megawatt reluctance synchronous wind generators. This thesis adds to the body of literature by successfully presenting and publishing two *IEEE* conference papers, from the contents of this thesis, that investigate how a simple, salient-pole reluctance synchronous wind generator compares to a published equivalent distributed flux-barrier RSG. The following conclusions are drawn:

- The salient-pole RSG has a high torque ripple. A distributed fractional-slot winding dramatically decreases this torque ripple to about 29% without negatively affecting the winding factor. Combining this fractional-slot winding with skewing further decrease the torque ripple, even to below 5%.
- Skew angles other than the conventional one slot-pitch can also be used to meet the design criteria. Investigating the skew angle as part of the design optimisation can present the design engineer with alternative designs. For the split-pole RSG a skew angle of two slot-pitches proves to be optimum.
- The novel torque equation can be used to get a first estimation and torque capability confirmation with about a 10% overestimation, for the salient-pole RSG.
- The biggest difference between the salient-pole RSG and the equivalent distributed flux-barrier RSG is the power factor. The power factor of the salient-pole RSG is about 37% lower than the distributed flux-barrier RSG.

- Splitting the rotor poles of the salient-pole RSG successfully improves the generator's low power factor. The power factor of the split-pole RSG is about 24% lower than the distributed flux-barrier RSG equivalent.

7.2 Recommendations

The following recommendations for future research are made:

- In order to establish whether using a salient-pole RSG design would be financially beneficial, the costs associated with both the distributed flux-barrier RSG system and the salient-pole RSG system should be calculated. The salient-pole RSG could potentially save on manufacturing costs, but would increase the costs associated with the synchronous rectifier side of the power electronic converter. A thorough cost comparison is thus recommended.

- Although the mechanical analysis shows that the proposed split-pole RSG structure is viable, a more thorough mechanical analysis is needed to find the optimum mechanical design. This final mechanical design should then also be optimised and would potentially provide more accurate simulated performance results.

- It is recommended that a scale model of the salient-pole and/or split pole RSG is designed, optimised, built and tested using the framework set up for this thesis. Although the results presented in this thesis are confirmed by two completely different FE-packages and solutions, the practical testing will increase the confidence in the accuracy of the simulation results and will provide a solid foundation for future work to be built on.

Appendices

Appendix A

Stress Analysis of the Split-pole RSG

Chapter 6 contains the results of a deformation analysis of the split-pole RSG. There, the initial split-pole RSG design is strengthened and a second deformation analysis is shown. In this appendix, the von Mises stresses of the unmodified split-pole RSG is shown in Figure A.1, with the area of greatest stress concentration shown in Figure A.2. The von Mises stresses of the strengthened split-pole RSG is shown in Figure A.3, with the area of greatest

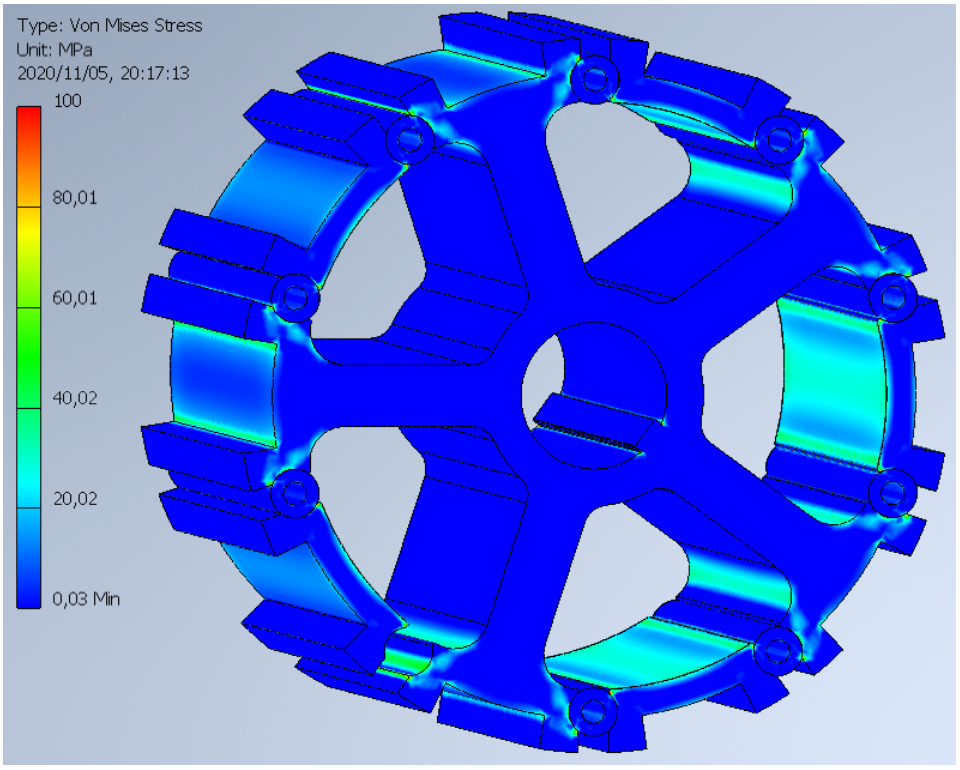

Figure A.1: Von Mises stress for the initial split-pole RSG design.

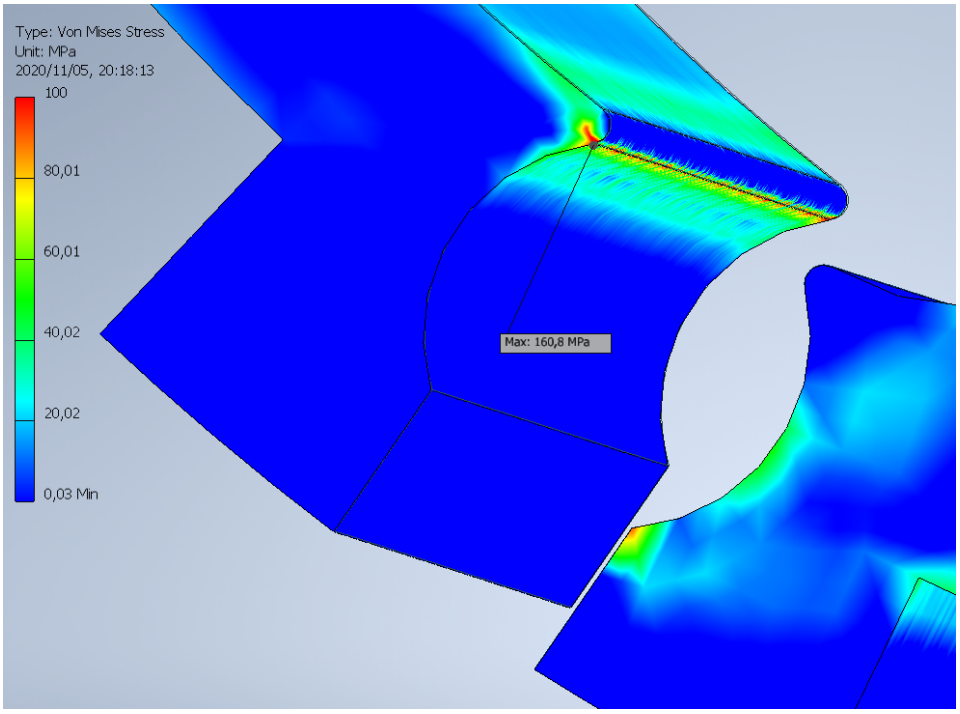

Figure A.2: Maximum stress region for the initial split-pole RSG design, with the cylindrical key removed.

stress concentration shown in Figure A.4.

The von Mises stress is used to determine if a material wil yield or fracture. For both of these designs, the von Mises stress is lower than that of steel. The highest stress occurs at the contact surface of the "floating" rotor pole, where it presses against the cylindrical key. The centrifugal force presses the bottom of the floating pole against the key, as shown in Figure A.2 and Figure A.4.

It is clear that the strengthening in Figure A.3 serves to generally decrease the stresses of the split-pole RSG design. The maximum stress of 192.2 MPa in Figure A.3 is higher than the maximum stress of 160.8 MPa for the unmodified RSG in Figure A.1. This is due to the increased weight of the design that provides the needed support to decrease the deformation, as discussed in Chapter 6.

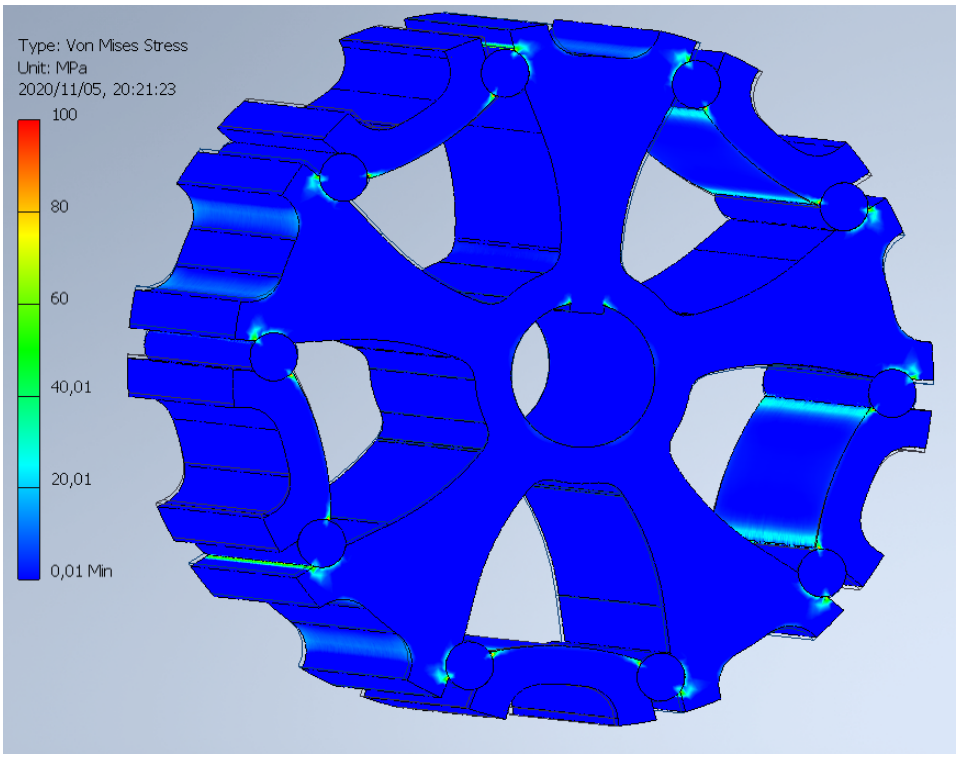

Figure A.3: Von Mises stress for the strengthened split-pole RSG design.

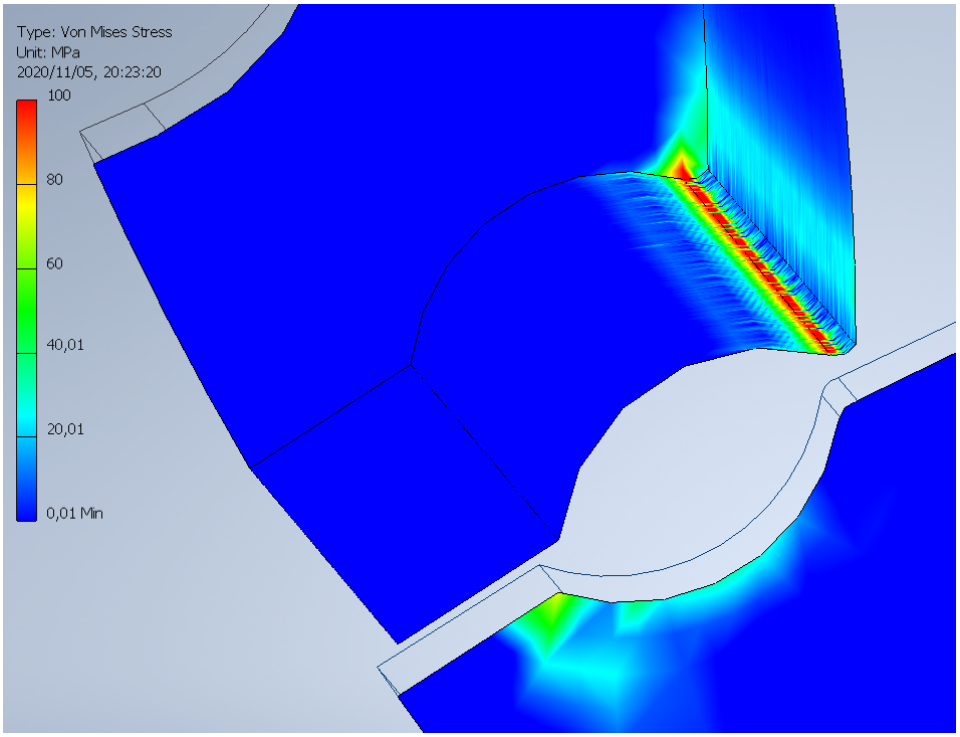

Figure A.4: Maximum stress region for the strengthened split-pole RSG design, with the cylindrical key removed.

List of References

[1] IEA: Offshore Wind outlook 2019. 2019.
Available at: https://www.iea.org/reports/offshore-wind-outlook-2019

[2] Yaramasu, V., Wu, B., Sen, P.C., Kouro, S. and Narimani, M.: High-power wind energy conversion systems: State-of-the-art and emerging technologies. *Proceedings of the IEEE*, vol. 103, no. 5, pp. 740–788, May 2015. ISSN 1558-2256.

[3] Holzer, T. and Muetze, A.: Full-size converter operation of large hydro power generators: Generator design aspects. In: *2018 IEEE Energy Conversion Congress and Exposition (ECCE)*, pp. 7363–7368. Sep 2018. ISSN 2329-3721.

[4] Wang, S., Nejad, A.R. and Moan, T.: On design, modelling, and analysis of a 10-MW medium-speed drivetrain for offshore wind turbines. *Wind Energy*. https://onlinelibrary.wiley.com/doi/pdf/10.1002/we.2476.
Available at: https://onlinelibrary.wiley.com/doi/abs/10.1002/we.2476

[5] IECRE: Wind energy, iecre certificates. 2020.
Available at: https://www.iecre.org/certificates/windenergy/

[6] Roshanfekr, P., Lundmark, S., Thiringer, T. and Alatalo, M.: A synchronous reluctance generator for a wind application-compared with an interior mounted permanent magnet synchronous generator. In: *7th IET International Conference on Power Electronics, Machines and Drives (PEMD 2014)*, pp. 1–5. April 2014. ISSN null.

[7] Howard, E. and Kamper, M.J.: Reluctance synchronous wind generator design optimisation in the megawatt, medium speed range. In: *2017 IEEE Energy Conversion Congress and Exposition (ECCE)*, pp. 1864–1871. Oct 2017.

[8] Botha, C.: *Variable Speed and Torque Control of a Wind Turbine System with Assisted Reluctance Synchronous Generator Technology*. MEng, Stellenbosch University, 2017.

[9] Kamper, M.: *Design Optimisation of Cageless Flux Barrier Rotor Reluctance Synchronous Machine*. PhD, Stellenbosch University, South Africa, 1996.

[10] Mitchell, J.: *The Control of a Back-to-back Power Converter for Small-Scale Reluctance Synchronous Generators in Grid-ConnectedWind Turbine Systems*. PhD, Stellenbosch University, 2017.

[11] Moghaddam, R.: *Synchronous Reluctance Machine (SynRM) in Variable Speed Drives (VSD) Applications*. PhD, KTH Royal Institute of Technology, 2011.

[12] Kostko, J.K.: Polyphase reaction synchronous motors. *Journal of the American Institute of Electrical Engineers*, vol. 42, no. 11, pp. 1162–1168, 1923.

[13] Taghavi, S. and Pillay, P.: A mechanically robust rotor with transverse-laminations for a synchronous reluctance machine for traction applications. In: *2014 IEEE Energy Conversion Congress and Exposition (ECCE)*, pp. 5131–5137. Sep 2014. ISSN 2329-3748.

[14] Howard, E.: *Design optimisation of Reluctance Synchronous Machines: A Motor and Generator Study*. PhD, Stellenbosch University, 2017.

[15] Sethuraman, L., Maness, M. and Dykes, K.L.: Optimized generator designs for the DTU 10-MW offshore wind turbine using generatorse: Preprint. In: *American Institute of Aeronautics and Astronautics 35th Wind Energy Symposium*. 2017.

[16] Ion Boldea and Syed A. Nasar: *The Induction Machine Handbook*. CRC Press, 2002.

[17] Howard, E., Kamper, M.J. and Gerber, S.: Asymmetric flux barrier and skew design optimization of reluctance synchronous machines. *IEEE Transactions on Industry Applications*, vol. 51, no. 5, pp. 3751–3760, 2015.

[18] Yu, H., Zhang, X., Ji, J. and Xu, L.: Rotor design to improve torque capability in synchronous reluctance motor. In: *2019 22nd International Conference on Electrical Machines and Systems (ICEMS)*, pp. 1–5. Aug 2019. ISSN 2640-7841.

[19] Constancias, R., Rasoanarivo, I., Takorabet, N. and Sargos, F.M.: Design and optimization of a synchronous reluctance machine with salient poles and flux barriers. In: *2010 IEEE Energy Conversion Congress and Exposition*, pp. 2672–2678. Sep 2010. ISSN 2329-3748.

[20] Motoranalysis - electric machine design and analysis software. `https://motoranalysis.com/`. Accessed: 2020-10-27.

[21] QuickField - electrical machines design. `https://quickfield.com/app_elmach.htm`. Accessed: 2020-10-27.

[22] Femm - finite element method magnetics. `http://www.femm.info/wiki/HomePage`. Accessed: 2020-10-27.

[23] ANSYS: Maxwell.
Available at: `https://www.ansys.com/products/electronics/ansys-maxwell`

[24] JMAG - simulation technology for electromechanical design. `https://www.jmag-international.com/`. Accessed: 2020-10-27.

[25] MagNet - 2D/3D electromagnetic field simulation software. https://www.mentor.com/products/mechanical/magnet/magnet/, .

[26] Comsol - AC/DC module. `https://www.comsol.com/acdc-module`. Accessed: 2020-10-27.

[27] MagneForce - simulation technology for rotating electric machines. `https://www.magneforcess.com/`, . Accessed: 2020-10-27.

[28] EMS - magnetic and electric field modeling software. `https://www.emworks.com/product/ems`. Accessed: 2020-10-27.

[29] Gerber, S.: *A finite element based optimisation tool for electrical machines*. Master's thesis, Stellenbosch University, South Africa, 2011.

[30] Gerber, S., Strauss, J.M. and Randewijk, P.J.: Evaluation of a hybrid finite element analysis package featuring dual air-gap elements. In: *The XIX International Conference on Electrical Machines - ICEM 2010*, pp. 1–6. 2010.

[31] Semfem documentation. `http://www0.sun.ac.za/semfem/v3/`. Accessed: 2020-10-25.

[32] Ansys. `https://www.ansys.com/`. Accessed: 2020-10-25.

[33] Bianchi, N., Bolognani, S., Pre, M.D. and Grezzani, G.: Design considerations for fractional-slot winding configurations of synchronous machines. *IEEE Transactions on Industry Applications*, vol. 42, no. 4, pp. 997–1006, 2006.

[34] Bomela, X.B. and Kamper, M.J.: Effect of stator chording and rotor skewing on performance of reluctance synchronous machine. *IEEE Transactions on Industry Applications*, vol. 38, no. 1, pp. 91–100, 2002.

[35] Hubert, T., Reinlein, M., Kremser, A. and Herzog, H..: Torque ripple minimization of reluctance synchronous machines by continuous and discrete rotor skewing. In: *2015 5th International Electric Drives Production Conference (EDPC)*, pp. 1–7. 2015.

[36] Sanada, M., Hiramoto, K., Morimoto, S. and Takeda, Y.: Torque ripple improvement for synchronous reluctance motor using an asymmetric flux barrier arrangement. *IEEE Transactions on Industry Applications*, vol. 40, no. 4, pp. 1076–1082, 2004.

[37] Moghaddam, R., Magnussen, F. and Sadarangani, C.: Novel rotor design optimization of synchronous reluctance machine for low torque ripple. In: *2012 XXth International Conference on Electrical Machines*, pp. 720–724. 2012.

[38] Vagati, A., Pastorelli, M., Francheschini, G. and Petrache, S.C.: Design of low-torque-ripple synchronous reluctance motors. *IEEE Transactions on Industry Applications*, vol. 34, no. 4, pp. 758–765, 1998.

[39] Spargo, C.M., Mecrow, B.C. and Widmer, J.D.: Application of fractional slot concentrated windings to synchronous reluctance machines. In: *2013 International Electric Machines Drives Conference*, pp. 618–625. 2013.

[40] Vanderplaats R&D: Visualdoc. `http://www.vrand.com/products/visualdoc/`. Accessed: 2020-10-27.

[41] Vanderplaats R&D: Visualdoc, getting started examples manual, v8.0. 2017. Available at: `http://www.vrand.com/`

[42] Ptakh, G.K., Zvezdunov, D.A. and Mustafaev, R.R.: Selection of stator yoke height of traction switched reluctance motor. In: *2016 2nd International Conference on Industrial Engineering, Applications and Manufacturing (ICIEAM)*, pp. 1–4. 2016.

[43] Akuru, U.B. and Kamper, M.J.: Novel experimentation of a 10 kW geared medium-speed wound-field flux switching wind generator drive. In: *2018 IEEE Energy Conversion Congress and Exposition (ECCE)*, pp. 6492–6498. 2018.

[44] Rakgati, E.T., Kamper, M.J. and Le Roux, A.D.: Torque performance of optimally designed six-phase reluctance DC machine. In: *Conference Record of the 2006 IEEE Industry Applications Conference Forty-First IAS Annual Meeting*, vol. 3, pp. 1186–1192. 2006.

[45] Boldea, I., Tutelea, L.N. and Torac, I.: 10MW, 10rpm, 15Hz directly-driven reluctance synchronous generator system: preliminary design with key FEM validations. In: *2020 IEEE Energy Conversion Congress and Exposition (ECCE)*, pp. 1835–1840. 2020.

[46] Wang, K., Zhu, Z., Ombach, G., Koch, M., Zhang, S. and Xu, J.: Torque ripple reduction of synchronous reluctance machines: using asymmetric flux-barrier. *COMPEL*, vol. 34, no. 1, pp. 18–31, Jan 2015. ISSN 0332-1649.
Available at: `https://doi.org/10.1108/COMPEL-11-2013-0367`

[47] Tahi, S., Ibtiouen, R. and Bounekhla, M.: Design optimization of two synchronous reluctance machine structures with maximized torque and power factor. *Progress In Electromagnetics Research B*, vol. 35, pp. 369–387, 01 2011.

[48] Stipetic, S., Zarko, D. and Cavar, N.: Adjustment of rated current and power factor in a synchronous reluctance motor optimally designed for maximum saliency ratio. *IEEE Transactions on Industry Applications*, vol. 56, no. 3, pp. 2481–2490, 2020.

[49] McDonald, A.S.: *Structural analysis of low speed, high torque electrical generators for direct drive renewable energy converters.* PhD, The University of Edinburgh, 2008.

[50] Wrobel, R. and Mecrow, B.C.: A comprehensive review of additive manufacturing in construction of electrical machines. *IEEE Transactions on Energy Conversion*, pp. 1–1, 2020. ISSN 1558-0059.

[51] Autodesk inventor. https://www.autodesk.com/products/inventor/.